LAWRENCE
LIVERMORE
NATIONAL
LABORATORY

LLNL-JRNL-401571

OXYGEN ISOTOPIC COMPOSITIONS OF THE ALLENDE TYPE C CAIs: EVIDENCE FOR ISOTOPIC EXCHANGE DURING NEBULAR MELTING AND ASTEROIDAL THERMAL METAMORPHISM

A. N. Krot, M. Chaussidon, H. Yurimoto, N. Sakamoto, K. Nagashima, I. D. Hutcheon, G. J. MacPherson

February 22, 2008

Geochimica et Cosmochimica Acta

Disclaimer

OXYGEN ISOTOPIC COMPOSITIONS OF THE ALLENDE TYPE C CAIs: EVIDENCE FOR ISOTOPIC EXCHANGE DURING NEBULAR MELTING AND ASTEROIDAL THERMAL METAMORPHISM

A. N. Krot[1*], M. Chaussidon[2], H. Yurimoto[3], N. Sakamoto[3], K. Nagashima[1], I. D. Hutcheon[4] and G. J. MacPherson[5]

[1]Hawai'i Institute of Geophysics and Planetology, School of Ocean and Earth Science and Technology, University of Hawai'i at Manoa, Honolulu, HI 96822, USA. *sasha@higp.hawaii.edu

[2]Centre de Recherches Pétrographiques et Géochimiques, CNRS-UPR 2300, BP20, 54501 Vandoeuvre les Nancy, France

[3]Division of Earth and Planetary Sciences, Hokkaido University, Sapporo 060-0810, Japan

[4]Glenn T. Seaborg Institute, Lawrence Livermore National Laboratory, Livermore, CA 94451, USA

[5]Smithsonian Institution, Department of Mineral Sciences, NHB 119, Washington DC 20560, USA

ABSTRACT. Based on the mineralogy and petrography, coarse-grained, igneous, anorthite-rich (Type C) calcium-aluminum-rich inclusions (CAIs) in the CV3 carbonaceous chondrite Allende have been recently divided into three groups: (*i*) CAIs with melilite and Al,Ti-diopside of massive and lacy textures (coarse grains with numerous rounded inclusions of anorthite) in a fine-grained anorthite groundmass (*6-1-72*, *100*, *160*), (*ii*) CAI *CG5* with massive melilite, Al,Ti-diopside and anorthite, and (*iii*) CAIs associated with chondrule material: either containing chondrule fragments in their peripheries (*ABC, TS26*) or surrounded by chondrule-like, igneous rims (*93*) (Krot et al., 2007a,b). Here, we report *in situ* oxygen isotopic measurements of primary (melilite, spinel, Al,Ti-diopside, anorthite) and secondary (grossular, monticellite, forsterite) minerals in these CAIs. Spinel ($\Delta^{17}O$ = –25‰ to –20‰), massive and lacy Al,Ti-diopside ($\Delta^{17}O$ = –20‰ to –5‰) and fine-grained anorthite ($\Delta^{17}O$ = –15‰ to –2‰) in *100*, *160* and *6-1-72* are ^{16}O-enriched relative spinel and coarse-grained Al,Ti-diopside and anorthite in *ABC*, *93* and *TS26* ($\Delta^{17}O$ ranges from –20‰ to –15‰, from –15‰ to –5‰, and from –5‰ to 0‰, respectively). In *6-1-72*, massive and lacy Al,Ti-diopside grains are ^{16}O-depleted ($\Delta^{17}O \sim -13$‰) relative to spinel ($\Delta^{17}O$ = –23‰). Melilite is the most ^{16}O-depleted mineral in all Allende Type C CAIs. In CAI *100*, melilite and secondary grossular, monticellite and forsterite (minerals replacing melilite) are similarly ^{16}O-depleted, whereas grossular in CAI *160* is ^{16}O-enriched ($\Delta^{17}O$ = –10‰ to –6‰) relative to melilite ($\Delta^{17}O$ = –5‰ to –3‰). We infer that CAIs *100*, *160* and *CG5* experienced melting in an ^{16}O-rich ($\Delta^{17}O \leq -20$‰) nebular gas in the CAI-forming region. The Type C and Type-B-like portions of CAI *6-1-72* experienced melting in an ^{16}O-depleted ($\Delta^{17}O \sim -13$‰) nebular gas. CAIs *ABC*, *TS26* and *93* experienced isotopic exchange during re-melting in the presence of an ^{16}O-poor ($\Delta^{17}O \geq -10$‰) nebular gas in the chondrule-forming region(s). Subsequently, Allende Type C CAIs experienced post-crystallization isotopic exchange with an ^{16}O-poor reservoir that affected largely melilite and anorthite. Because pseudomorphic replacement of lacy melilite by grossular, monticellite and forsterite occurred during thermal metamorphism, some oxygen isotopic exchange of melilite and anorthite must have continued after formation of these secondary minerals. We suggest that some or all oxygen isotopic exchange in melilite and anorthite occurred during fluid-assisted thermal metamorphism on the CV parent asteroid. Similar processes may have also affected melilite and anorthite of CAIs in metamorphosed CO chondrites.

submitted to *Geochimica et Cosmochimica Acta* March 5, 2007
revised June 14, 2007

INTRODUCTION

Most CAIs in primitive chondrites (e.g., CR2, CO3.0 and the ungrouped carbonaceous chondrite Acfer 094) have uniformly ^{16}O-rich ($\Delta^{17}O \leq -20‰$) compositions (Aléon et al., 2002; Itoh et al., 2004; Fagan et al., 2007) and show large excesses of ^{26}Mg [^{26}Mg* – decay product of a short-lived ($t_{1/2}$ = 0.73 Myr) radionuclide ^{26}Al], indicating early formation in an ^{16}O-rich gaseous reservoir (e.g., MacPherson et al., 1995; Krot et al., 2002). Few CAIs in these meteorites subsequently experienced melting and isotopic exchange in the presence of an ^{16}O-poor nebular gas (Aléon et al., 2002; Itoh et al., 2004; Krot et al., 2005a). In contrast, most CV CAIs, which appear to have formed very early (Amelin et al., 2002), during a short time interval (Thrane et al., 2006), show large oxygen isotopic heterogeneity: melilite and anorthite are typically ^{16}O-depleted ($\Delta^{17}O > -10‰$) compared to spinel and Al,Ti-diopside, which largely retain their original, ^{16}O-rich compositions (e.g., Clayton et al., 1977; McKeegan et al., 1998; Aléon et al., 2005a,b). Because some melilite and anorthite grains in the Allende CAIs have ^{16}O-rich compositions (e.g., Yurimoto et al., 1998; Yoshitake et al., 2002; Harazono and Yurimoto, 2003; Kim et al., 2002; Ito et al., 2004; Fagan et al., 2004; Aléon et al., 2005b), isotopic exchange with an ^{16}O-poor external reservoir is required.

Several mechanisms have been proposed to explain the nature of this selective isotopic exchange, but all have some problems. (*i*) High-temperature gas-solid exchange in the solar nebula (Clayton et al., 1977) is inconsistent with the measured oxygen self-diffusion rates in melilite, anorthite, diopside and spinel (Yurimoto et al., 1989; Ryerson and McKeegan, 1994). (*ii*) Isotopic exchange between the ^{16}O-rich CAI melt and an ^{16}O-poor nebular gas either during CAI melting or crystallization is difficult to reconcile with the inferred crystallization sequence of CAI melts (Stolper, 1982; Stolper and Paque, 1986). (*iii*) Isotopic exchange during disequilibrium melting (Yurimoto et al., 1998; Greenwood, 2004) might avoid these problems, but has yet to be reproduced experimentally. (*iv*) Isotopic exchange during relatively low-temperature alteration in the presence of fluid phase either on the CV parent asteroid or in the solar nebula has been advocated by several researchers (e.g., Krot et al., 1998; Jabeen et al., 1998a,b, 1999; Ash et al., 1999; Ash and Young, 2000; Young et al., 1999; Harazono and Yurimoto, 2003). However, the lack of experimental data on the diffusion rates of oxygen in CAI-like minerals in the presence of aqueous solution does not allow to test this hypothesis yet.

Most isotopically heterogeneous CAIs in CV chondrites are surrounded by multilayered Wark-Lovering rims; some are also surrounded by coarse-grained, forsterite-rich, accretionary rims (e.g., Krot et al., 2001; Cosarinsky et al., 2002). The outermost layers of the Wark-Lovering rims composed of spinel and Al,Ti-diopside, and forsterite of the accretionary rims are ^{16}O-enriched to the same level as spinel and Al,Ti-diopside of their host CAIs, whereas anorthite and melilite rim layers are generally ^{16}O-depleted (McKeegan et al., 1998; Krot et al., 2002; Cosarinsky et al., 2002; Yoshitake et al., 2002). Since it is generally accepted that Wark-Lovering rims resulted from high-temperature gas-solid or gas-melt interaction (e.g., MacPherson, 2003 and references therein), whereas forsterite of the accretionary rims directly condensed from the nebular gas (e.g., Petaev and Wood, 2005), these observations require formation of the rims (i.e., final stages of CAI formation) in the presence of ^{16}O-rich nebular gas. If oxygen isotopic heterogeneity of CV CAIs resulted from gas-melt isotopic exchange in the solar nebula, rapid fluctuations of oxygen isotopic compositions of the nebular gas (from ^{16}O-rich to ^{16}O-poor to ^{16}O-rich again) are required (Yurimoto et al., 1998; Itoh and Yurimoto, 2003).

We have recently shown that coarse-grained, igneous, anorthite-rich (Type C) CAIs from Allende experienced complex formation histories, involving multiple episodes of nebular melting and post-crystallization alteration, probably in an asteroidal setting (Krot et al., 2005b, 2007a,b). Several Allende Type C CAIs (*ABC*, *TS26*, 93) were re-melted with addition of ferromagnesian silicates in the chondrule-forming region, characterized by ^{16}O-poor composition of the nebular gas (Krot et al., 2005b, 2007a). We note that oxygen isotopic compositions of the Allende Type C CAIs are largely unknown. Imai and Yurimoto (2000) described mineralogy, magnesium and oxygen isotopic compositions of an extensively altered Type C CAI (*TTA-01*). The CAI shows oxygen isotopic heteregeneity: the mean values of δ^{17}O and δ^{18}O for spinel, melilite, anorthite and nepheline are (–46‰, –45‰), (+5‰, +12‰), (+5‰, +9‰) and (+2‰, +5‰), respectively. Imai and Yurimoto (2000) identified two textural types of Al,Ti-diopside in the CAI – coarse-grained and fine-grained. The coarse-grained Al,Ti-diopside is ^{16}O-enriched (δ^{17}O = –35‰, δ^{18}O = –31‰) relative to the fine-grained (δ^{17}O = +6‰, δ^{17}O = +17‰). Magnesium isotopic compositions of melilite plot along the canonical ^{26}Al/^{27}Al ratio of 5×10^{-5}, whereas those of anorthite are distributed between the slopes of 0 and 5×10^{-5}, indicative of late-stage disturbance. Based on these observations, Imai and Yurimoto (2000) concluded that CAI *TTA-01* experienced oxygen isotopic exchange during remelting.

In order to understand the role of nebular melting and asteroidal processing in oxygen isotopic exchange of the CV CAIs, we measured oxygen isotopic compositions of seven Allende Type Cs – *100*, *160*, *6-1-72*, *CG5*, *ABC*, *TS26* and *93*. The mineralogy, petrography, bulk chemical compositions and trace element abundances of these CAIs have been previously reported by Wark (1987) and Krot et al. (2005b, 2007a,b).

ANALYTICAL TECHNIQUES

Polished thin and thick sections of the Allende Type C CAIs *160*, *100*, *6-1-72*, *CG5*, *93*, *ABC* and *TS26* were studied using optical microscopy, X-ray elemental mapping, backscattered electron (BSE) imaging, electron probe microanalysis (EPMA), and secondary ion mass-spectrometry (SIMS). The BSE images were obtained with a JEOL JSM-5900LV scanning electron microscope equipped with Thermo Electron energy dispersive spectrometer (EDS) using a 15-20 kV accelerating voltage and 1-2 nA beam current. X-ray elemental maps with a resolution of 1-10 μm/pixel were acquired using five spectrometers of a Cameca SX-50 microprobe at 15 keV accelerating voltage, 50-100 nA beam current and ~1-2 μm beam size. The elemental maps in Mg, Ca and Al Kα were combined using a RGB-color scheme and ENVI (ENvironment for Visualizing Images) software package. Electron probe microanalyses were performed with a Cameca SX-50 electron microprobe using a 15 keV accelerating voltage, 10-20 nA beam current, beam size of ~1-2 μm and wavelength dispersive X-ray spectroscopy. For each element, counting times on both peak and background were 30 sec (10 sec for Na and K). Bulk compositions of chondrules were measured using a defocused ~10 μm beam. Matrix effects were corrected using the PAP procedure (Pouchou and Pichoir, 1984). The detection limits were (in wt%): SiO_2, Al_2O_3, MgO, CaO, 0.03; TiO_2, Cr_2O_3, 0.04; K_2O, 0.04; Na_2O, 0.06; MnO, FeO, 0.07.

Oxygen isotopic compositions were measured *in situ* using the CRPG-CNRS (Nancy) and Hokkaido University (HU) Cameca ims 1270 ion microprobes and University of Hawai‘i (UH) Cameca ims 1280 ion microprobe.

In Nancy, oxygen isotopic data were collected in multicollection mode. ^{16}O and ^{18}O were measured using Faraday cups (FC); ^{17}O was measured using the axial electron multiplier (EM). A Cs^+ primary beam of 10 nA was used to produce ion probe sputter pits approximately 25-30 μm in diameter. With such conditions, the count rate was ~2×10^6 sec^{-1} for ^{18}O. Corrections for instrumental mass fractionation (IMF), counting statistics, and uncertainty in standard

compositions were applied. The IMF was corrected using terrestrial standards: San Carlos olivine and diopside (for details, see Gurenko and Chaussidon, 2002). Under the analytical conditions employed, the precision (2σ) of individual oxygen isotopic analyses is better than 1.5‰ for both $\delta^{18}O$ and $\delta^{17}O$.

At HU, a primary ion beam of mass filtered Cs^+ ions accelerated to 20 keV was used to excavate shallow pits ranging from 3 to 10 μm across. The primary current was adjusted for each measurement to obtain a count rate for $^{16}O^-$ ions of ~3.5 to 4×10^5 sec^{-1}. A normal-incidence electron gun was used for charge compensation of analyzed areas. Negative secondary ions from the $^{16}O^-$ tail, $^{16}O^-$, $^{17}O^-$, $^{16}OH^-$ and $^{18}O^-$ were analyzed at a mass resolving power (m/Δm) of ~6000, sufficient to completely separate $^{16}OH^-$ interference on $^{17}O^-$. Secondary ions were detected by a monocollector EM in pulse counting mode, and analyses were corrected for dead time. The IMF was corrected using terrestrial standards: SPU spinel (from Russia), anorthite (Miyake-jima, Japan), augite (Takashima, Japan), and synthetic gehlenite and åkermanite. The reproducibility of $^{17}O/^{16}O$ and $^{18}O/^{16}O$ on different analysis points from the same standard was ~ ±5‰ (2σ). Matrix effects on detected oxygen isotopic compositions among the minerals analyzed are also limited to about ±5‰. Therefore, we used one standard, the SPU spinel, to determine IMF during each analytical session.

At UH, a 2-3 nA focused Cs^+ primary ion beam was rastered over a 25×25 micron area for 120-150 seconds. Then the raster was reduced to 10×10 microns and data collected for 4 sec × 40 cycles. The secondary ion mass spectrometer was operated at −10 keV with a 50 eV energy window. $^{16}O^-$ was measured on multicollector FC L'2 with 10^{10} ohm resistor; $^{18}O^-$ was measured on FC H1 with 10^{11} ohm resistor, and $^{17}O^-$ was measured with the monocollector EM. The mass resolving power for $^{16}O^-$ and $^{18}O^-$ was ~2000, and that for $^{17}O^-$ was ~5500, sufficient to separate interfering $^{16}OH^-$. The normal-incidence electron flood gun was used for charge compensation. All data were corrected for IMF using synthetic forsterite and olivine from the Brenham pallasite. Under the analytical conditions employed, the total precision (2σ) of individual oxygen isotopic analyses is ~1.5‰ for both $\delta^{18}O$ and $\delta^{17}O$. We note that IMF for spinel, Al,Ti-diopside, anorthite and melilite could be different for the UH Cameca ims-1280 (e.g., Kita et al., 2007), which would result in larger uncertainty in $\delta^{18}O$.

Oxygen isotopic compositions are reported as per mil deviations from SMOW (Standard Mean Ocean Water) ($\delta^{18}O$ and $\delta^{17}O$) and as ^{16}O excesses relative to terrestrial samples ($\Delta^{17}O$).

Following oxygen isotopic measurements, each CAI analyzed was re-examined in BSE and secondary electron images to verify the locations of the sputtered craters and mineralogy of the phases analyzed.

SAMPLE DESCRIPTION

The detailed mineralogy and petrography of the Allende Type C CAIs have been described by Wark (1987) and Krot et al. (2007a,b). Here, we just briefly summarize the major mineralogical characteristics of these CAIs important for understanding their oxygen isotopic compositions. Additional X-ray elemental maps illustrating overall mineralogy of the CAIs are included in an electronic annex (EA).

Based on the mineralogy and petrography, Type C CAIs from Allende have been divided into three groups:

(1) CAIs with melilite and Al,Ti-diopside of massive and lacy textures (coarse grains with numerous rounded inclusions of anorthite; Wark, 1987) in a fine-grained anorthite groundmass (*6-1-72*, *100*, *160*),

(2) CAI *CG5* with massive melilite, Al,Ti-diopside and anorthite, and

(3) CAIs associated with chondrule material – either containing chondrule fragments in their peripheries (*ABC, TS26*) or surrounded by chondrule-like, igneous rims (*93*) (Krot et al., 2007a,b).

160 is a fragmented CAI partly surrounded by a Wark-Lovering rim sequence of spinel, Al,Ti-diopside and olivine (Figs. 1EA, 1). The CAI is composed of Al,Ti-diopside, melilite, spinel and fine-grained, anorthite groundmass. Al,Ti-diopside occurs as lacy grains, as rare massive grains poikilitically enclosing euhedral spinel, and as interstitial grains between polycrystalline melilite. Melilite occurs as lacy grains and as compact, polycrystalline regions. Lacy melilite grains are pseudomorphed to varying degrees by grossular, monticellite and forsterite. Melilite and anorthite in the outer portion of the CAI are extensively replaced by nepheline and sodalite.

100 consists of four CAI fragments (hereafter "*100a*", "*100b*", "*100c*" and "*100d*") (Figs. 2EA, 3). The petrographic context of the fragments is unknown; none of the CAI fragments have Wark-Lovering rim layers. All four CAI fragments consist of melilite, Al,Ti-diopside, spinel and fine-grained, anorthite groundmass; they show, however, significant variations in the morphology of Al,Ti-diopside and melilite grains among the fragments. Al,Ti-diopside occurs as coarse (100-200 μm in size) euhedral grains with lacy textures and as nearly anorthite-free small (20-30 μm in size) isolated crystals or their aggregates. Most melilite grains have lacy textures. Anorthite-free, massive melilite regions are rare and are overgrown by lacy melilite and lacy Al,Ti-diopside; the former are pseudomorphed to varying degrees by grossular, monticellite and forsterite.

6-1-72 is a complete, ellipsoid CAI surrounded by a Wark-Lovering rim sequence of spinel, Al,Ti-diopside and olivine (Figs. 3EA, 5), and consisting of two texturally distinct regions. The main portion is mineralogically similar to CAIs *100* and *160*. It is composed of fine-grained groundmass anorthite and coarse-grained, lacy Al,Ti-diopside and melilite; spinel is relatively minor and heterogeneously-distributed in the CAI. Lacy melilite is pseudomorphed by grossular, monticellite and forsterite. The CAI core is free of nepheline and sodalite; both minerals, however, are common in the periphery, where they replace anorthite and, possibly, melilite. The core is heavily fractured; some of the fractures are filled by andradite and wollastonite. The other portion of *6-1-72* consists of compact, polycrystalline melilite, Al,Ti-diopside, isolated spinel grains and a spinel palisade body. Melilite and Al,Ti-diopside contain abundant inclusions of spinel, perovskite and platinum group element nuggets; neither melilite nor Al,Ti-diopside have lacy texture. Melilite along grain boundaries is replaced by grossular, monticellite and forsterite. Coarse-grained melilite and the palisade body are overgrown by lacy Al,Ti-diopside. This portion is texturally and mineralogically similar to Type B CAIs from CV chondrites (e.g., MacPherson et al., 1988).

CG5 is a CAI fragment composed of lath-shaped anorthite, Al,Ti-diopside and melilite, all poikilitically enclosing abundant spinel grains; secondary minerals and Wark-Lovering rim layers are absent (Figs. 4EA, 7). Melilite and Al,Ti-diopside occur in interstitial regions between prismatic anorthite crystals and also form large, massive grains in anorthite-poor regions of the CAI.

93 is a CAI fragment composed of coarse-grained, Al,Ti-diopside, lath-shaped anorthite, euhedral Cr-bearing spinel and interstitial, fine-grained regions composed of melilite, Al-diopside and anorthite (Fig. 9). In the core, coarse-grained anorthite is largely replaced by nepheline and sodalite, while in the periphery, anorthite is replaced by sodalite, ferrous olivine and nepheline. The interstitial melilite-anorthite-diopside intergrowth is replaced by a fine-grained, porous material largely composed of grossular, monticellite and wollastonite; minor secondary nepheline and sodalite occur as well. The peripheral zone of the CAI is overgrown by a coarse-grained igneous region composed of augite, pigeonite and anorthitic plagioclase. Plagioclase is extensively replaced by sodalite and ferrous olivine. The coarse-grained, igneous region is separated from the CAI by a spinel-rich layer, possibly a remnant of a Wark-Lovering rim.

ABC is a CAI fragment composed of lath-shaped anorthite and Al,Ti-diopside, both poikilitically enclosing spinel grains, and fine-grained, interstitial material (Fig. 11). Anorthite is corroded by sodalite and nepheline. The interstitial material consists of melilite, Al-diopside, grossular, wollastonite and monticellite. Relict olivine and low-Ca pyroxene grains occur in the peripheral portion of the fragment.

TS26 is a complete, irregularly-shaped CAI that shows a well-defined core-mantle structure (Figs. 5EA, 13). The coarse-grained core consists of lath-shaped anorthite and euhedral, sector-zoned Al,Ti-diopside, both poikilitically enclosing spinel grains, and interstitial material. The interstitial material is composed of melilite, diopside and secondary grossular, monticellite, wollastonite, sodalite and ferrous olivine; the secondary minerals replace melilite and anorthite. The mantle is finer-grained and enriched in SiO_2 compared to the core. It is separated from the core by a discontinuous layer of Fe,Ni-sulfides and composed of Al,Ti-diopside, lath-shaped anorthite and abundant relict grains of forsteritic olivine and low-Ca pyroxene. The olivine and low-Ca pyroxene grains are extensively corroded by diopside and surrounded by haloes of augite; augite is also present in the outermost portion of the mantle.

OXYGEN ISOTOPIC COMPOSITIONS

Type C CAIs with melilite and Al,Ti-diopside of massive and lacy textures

In CAI *160* (Fig. 1), oxygen isotopes were measured in both lacy and massive textural types of melilite and Al,Ti-diopside, as well as spinel, anorthite groundmass and a fine-grained mixture of grossular+monticellite replacing lacy melilite (Table 1, Fig. 2). In Fig. 2a, the data are plotted as $\delta^{17}O$ *vs.* $\delta^{18}O$. To illustrate variations in oxygen isotopic compositions of individual minerals, in Fig. 2b, the same data, grouped by minerals, are plotted as $\Delta^{17}O = \delta^{17}O - 0.52\times\delta^{18}O$. Spinel and massive Al,Ti-diopside grains are similarly ^{16}O-enriched ($\Delta^{17}O$ = –24‰ to –23‰) relative to lacy Al,Ti-diopside ($\Delta^{17}O$ = –20‰ to –17‰). The apparent ^{16}O-depletion of lacy Al,Ti-diopside is probably due to small inclusions of ^{16}O-depleted anorthite, which shows a wide compositional range ($\Delta^{17}O$ = –10‰ to –2‰). Massive melilite and lacy melilite have similar, ^{16}O-poor compositions ($\Delta^{17}O$ = –5‰ to –3‰). The grossular-monticellite intergrowths are ^{16}O-enriched ($\Delta^{17}O$ = –10‰ to –6‰) relative to the lacy melilite they replace.

In CAI *100* (Fig. 3), oxygen isotopes were measured in two textural types of melilite (lacy and massive), three textural occurrences of Al,Ti-diopside (lacy, small euhedral grains and a compact aggregate of grains), spinel, anorthite groundmass and secondary forsterite, monticellite

and grossular using the CNRS/CRPG and HU ion microprobes (Table 1, Fig. 4). Although there is a reasonable agreement between the two data sets, they have different error bars and are plotted separately (Fig. 4). Lacy Al,Ti-diopside grains are slightly ^{16}O-depleted (Δ^{17}O = –18‰ to –17‰) relative to ^{16}O-rich (Δ^{17}O = –25‰) spinel. These Al,Ti-diopsides are compositionally similar to small, euhedral Al,Ti-diopside grains (Δ^{17}O = –21‰ to –16‰) and to a compact aggregate of small Al,Ti-diopside grains (Δ^{17}O = –18‰). The observed range in oxygen isotopic composition of Al,Ti-diopside and the slight ^{16}O-depletion are probably due to small anorthite grains sputtered during ion probe analyses together with Al,Ti-diopside (see, e.g., spots 87, 88, 92 and 93 in Figs. 3a-c). Although ion probe analyses of pure Al,Ti-diopside collected by the HU ims-1270 show relatively large spread in Δ^{17}O (–23‰ to –15‰), these analyses have large error bars (±5‰, 2σ) and within 2σ error can be considered similar (Figs. 4c,d). Fine-grained anorthite shows a wide compositional range (Δ^{17}O = –14‰ to –4‰), even if we ignore the spots contaminated by tiny inclusions of spinel and Al,Ti-diopside (Table 1). Massive (Fig. 3d) and lacy (Fig. 3e) melilite have similar, ^{16}O-poor compositions (Δ^{17}O = –5‰ to –3‰). Secondary grossular, monticellite and forsterite – minerals replacing lacy melilite (Figs. 3d-f) – have ^{16}O-poor compositions (Δ^{17}O = –9‰, –2‰, and –3‰ to –5‰, respectively; ±5‰ 2σ errors), comparable with melilite.

In CAI *6-1-72*, oxygen isotopic compositions were measured for the Type B-like and Type C portions (Figs. 5, 6). Lacy Al,Ti-diopside and melilite of the Type C portion (Figs. 5a,b) show similar ranges of oxygen isotopic compositions (Δ^{17}O = –13‰ to –6‰). Although fine-grained anorthite shows a wider compositional range (Δ^{17}O = –14‰ to –1‰), most analyses are contaminated by small interstitial grains of Al,Ti-diopside (Figs. 5a,b). Four clean analyses of anorthite have a narrower compositional range (Δ^{17}O = –8‰ to –1‰), with the most ^{16}O-depleted composition (spot 32, Table 1) observed near the CAI periphery (Fig. 5c), where anorthite is extensively replaced by nepheline and sodalite. In the Type B-like portion (Figs. 5d-f), massive Al,Ti-diopside grains are ^{16}O-depleted (Δ^{17}O = –14‰ to –6‰) relative to spinel (Δ^{17}O = –23‰). The entire compositional range of Al,Ti-diopside is due to three analyses collected by the CNRS/CRPG ion probe which are contaminated either by melilite or spinel (Fig. 5d). Three analyses of Al,Ti-diopside collected at UH are free of inclusions of other minerals (Fig. 5e) and show a much narrower compositional range (Δ^{17}O = –13‰ to –12‰), which can be

considered as representative of the *6-1-72* Al,Ti-diopside. Oxygen isotopic analyses of melilite, contaminated to varying degrees by grossular and monticellite (Fig. 5f), range in composition from –7‰ to –2‰ ($\Delta^{17}O$); the cleanest analyses of melilite (an. 19, 20, Fig. 5e) have $\Delta^{17}O$ = –7‰.

Type C CAI CG5 with massive melilite and Al,Ti-diopside

CAI *CG5* is highly enriched in spinel (Fig. 7). As a result, all ion probe analyses of *CG5* are contaminated by spinel (Table 1, Fig. 8). Melilite+spinel and anorthite+spinel spots are ^{16}O-depleted relative to Al,Ti-diopside+spinel ($\Delta^{17}O$ = –12‰ to –11‰, –15‰ to –8‰, and –23‰, respectively), indicating that spinel and Al,Ti-diopside are ^{16}O-enriched relative to anorthite and melilite.

Type C CAIs with chondrule-like, igneous rims or chondrule fragments in their peripheries

In CAI *93*, overgrown by a chondrule-like, igneous rim (Fig. 9), spinel shows the highest enrichment in ^{16}O ($\Delta^{17}O$ = –16‰; Table 1, Fig. 10). Al,Ti-diopside is ^{16}O-depleted ($\Delta^{17}O$ = –11‰ to –8‰), while anorthite and melilite are ^{16}O-poor ($\Delta^{17}O$ = –2‰ and –1‰, respectively) (Table 1, Fig. 10). The oxygen isotopic composition of augite in the coarse-grained, igneous rim is slightly ^{16}O-depleted ($\Delta^{17}O$ = –8‰ to –5‰) compared to that of Al,Ti-diopside in the host CAI.

In CAI fragment *ABC* (Figs. 11a,b), relict grains of olivine and low-Ca pyroxene (Fig. 11c) have ^{16}O-poor compositions ($\Delta^{17}O$ = –6‰ and –4‰, respectively; Table 1, Figs. 12a,b). Spinel and Al,Ti-diopside are moderately ^{16}O-enriched ($\Delta^{17}O$ down to –16‰). Al,Ti-diopside shows a wide compositional range ($\Delta^{17}O$ = –16‰ to –6‰); both the highest and the lowest values of $\Delta^{17}O$ were found in the CAI portion containing relict grains of olivine and low-Ca pyroxene. Chromian spinel ($\Delta^{17}O$ = –11‰), anorthite ($\Delta^{17}O$ = –5‰ to –1‰) and melilite ($\Delta^{17}O$ = +2‰) are ^{16}O-depleted to varying degrees (Table 1, Figs. 12a,b).

In CAI *TS26* (Fig. 13a-c), spinel ($\Delta^{17}O$ = –20‰ to –19‰) and anorthite ($\Delta^{17}O$ = –3‰ to –1‰) have the lightest and the heaviest O-isotopic compositions, respectively (Table 1, Figs. 12c,d). We note, however, that melilite has not been analyzed in this CAI. Al,Ti-diopside grains show a wide compositional range ($\Delta^{17}O$ = –15‰ to –3‰). Al,Ti-diopside grains in the CAI core are ^{16}O-enriched ($\Delta^{17}O$ = –15‰ to –10‰) compared to those in the CAI mantle ($\Delta^{17}O$ = –5‰ to

–3‰). Augite and relict olivine (Fig. 13d) have ^{16}O-poor compositions (Δ^{17}O = –8‰ and –1‰, respectively).

DISCUSSION

Oxygen isotopic exchange during melting of the Allende Type C CAIs

The Type C CAIs described above preserve an ^{16}O-rich isotopic signature in some of their primary, high-temperature minerals, suggesting they all were initially ^{16}O-rich, like the majority of CAIs from primitive chondrites, i.e., Δ^{17}O $\leq$ –20‰ (e.g., Aléon et al., 2002; Itoh et al., 2004; Fagan et al., 2007). The observed ^{16}O-depletion of some primary minerals in these CAIs must have resulted from subsequent isotopic exchange.

CAIs 160, 100, 6-1-72 and CG5

Based on the mineralogical observations, we have previously suggested that (*i*) CAI *CG5* formed by melting of a fine-grained, spinel-rich CAI with melilite and spinel partially replaced by anorthite and diopside. (*ii*) CAIs *100*, *160* and *6-1-72* formed by remelting of coarse-grained, melilite-spinel-Al,Ti-diopside (Type B-like) CAIs which experienced either extensive replacement by anorthite and diopside prior to melting or addition of silica by gas-liquid condensation during melting (Krot et al., 2007b). This interpretation implies that CAIs *100*, *160* and *6-1-72* experienced at least two distinct melting events. Since CAIs *160* and *6-1-72* are surrounded by the Wark-Lovering rim layers, we inferred that the last melting event must have occurred in the CAI-forming region. CAIs *100* and *CG5* are completely fragmented and the presence or absence of rims around them prior to fragmentation can not be inferred from petrographic observations.

Massive and lacy Al,Ti-diopsides in *160, 100* and *CG5* are ^{16}O-rich (Δ^{17}O $\leq$ –20‰). Spinel in these CAIs is similarly ^{16}O-rich, while anorthite inclusions in lacy Al,Ti-diopside are ^{16}O-depleted (Figs. 2, 4, 8). We infer that spinel and massive and lacy Al,Ti-diopside in *100, 160* and *CG5* were melted in the presence of an ^{16}O-rich nebular gas in the CAI-forming region.

Massive Al,Ti-diopside of the Type-B-like portion and lacy Al,Ti-diopside (taking into account ^{16}O-depleted compositions of anorthite inclusions) of the Type C portion of *6-1-72* are similarly ^{16}O-depleted (Δ^{17}O ~ –13‰; only clean analyses of massive Al,Ti-diopside are considered) relative to spinel (Δ^{17}O < –20‰; Fig. 8). This suggests that Al,Ti-diopside of both

portions of *6-1-72* experienced melting and isotopic exchange in an ^{16}O-depleted ($\Delta^{17}O \sim -13‰$) nebular gas, whereas spinel is relict. The existence of such nebular gas during formation of igneous CAIs is consistent with the presence of the uniformly ^{16}O-depleted compositions ($\Delta^{17}O$ down to $\sim -15‰$) of Type B and compact Type A CAIs reported in CR carbonaceous chondrites (Aléon et al., 2002). Evidence for an early oxygen isotopic exchange during melting of a compact Type A CAI from Allende has been recently reported by Aléon et al. (2005b).

Fine-grained anorthite in *100, 160* and in Type C portion of *6-1-72* is ^{16}O-depleted relative to spinel and Al,Ti-diopside (Figs. 2, 4, 6). Anorthite shows a large range in oxygen isotopic compositions ($\Delta^{17}O$ from –15‰ to –2‰), with the lightest compositions (in *6-1-72*) overlapping with those of Al,Ti-diopside. The heaviest compositions of anorthite in all three CAIs overlap with those of melilite grains ($\Delta^{17}O$ from –6‰ to –3‰). These observations indicate that oxygen isotopic compositions of anorthite and melilite resulted from exchange that preferentially affected these two minerals. The nature of this exchange can be inferred from the oxygen isotopic compositions of secondary grossular, monticellite, ±forsterite, ±wollastonite forming pseudomorphs after melilite+anorthite in Type C CAIs (e.g., Figs. 1, 3) and from the O-isotopic compositions of melilite in the least metamorphosed CV chondrite Kaba (Nagashima et al., 2007) as discussed below.

CAIs 93, ABC and TS26

We have previously shown that Type C CAIs *93*, *ABC* and *TS26* experienced late-stage melting in the chondrule-forming regions with addition of ferromagnesian chondrule materials, probably coincident with chondrule formation (Krot et al., 2007a,b). Based on the oscillatory zoning of Al,Ti-diopsides in *ABC* and *93* (Fig. 11 in Krot et al., 2007a), and the enrichment in Cr_2O_3 and depletion in TiO_2 and Al_2O_3 relative to pyroxenes in typical Type B and Type C CAIs (Fig. 3 in Krot et al., 2007a), we concluded that pyroxenes in *ABC* and *93* experienced nearly complete melting. In contrast, in *TS26*, the degree of melting and mixing with chondrule material appears to decrease inward, towards the CAI core, as indicated by the differences in chemical compositions of the core and mantle pyroxenes (Fig. 3 in Krot et al., 2007a) and by a distinct boundary between the finer-grained mantle and the coarser-grained core clearly visible in transmitted light (Fig. 5EA) and the Si Kα X-ray map (Fig. 7b in Krot et al., 2007a).

Spinel and Al,Ti-diopside grains in CAIs *93*, *ABC* and in the mantle of *TS26* are ^{16}O-depleted to varying degrees (Δ^{17}O range from –16‰ to –3‰) (Table 1, Figs. 10, 12). Based on these observations, we infer that spinel and Al,Ti-diopside of *93* and *ABC* and Al,Ti-diopside in the mantle of *TS26* experienced oxygen isotopic exchange to varying degrees during melting event in the chondrule-forming region. Anorthite and melilite, which crystallized before and after Al,Ti-diopside, respectively, must have experienced oxygen isotopic exchange during this melting event as well.

Spinel in the core of *TS26* retained its initial ^{16}O-rich composition (Δ^{17}O = –20‰), whereas coarse Al,Ti-diopside grains are ^{16}O-depleted (Δ^{17}O = –15‰ to –10‰). These Al,Ti-diopside grains, however, are ^{16}O-enriched relative to Al,Ti-diopside in the CAI mantle (Δ^{17}O = –5‰ to –3‰; Fig. 12). These observations suggest that spinel in the CAI core is largely relict (i.e., escaped melting during formation of the igneous mantle), whereas Al,Ti-diopside experienced melting and isotopic exchange in an ^{16}O-poor nebular gas either during the event that produced the mantle or prior to it.

Coarse-grained, lath-shaped anorthite in *93*, *ABC* and *TS26* is ^{16}O-depleted relative to Al,Ti-diopside which crystallized after anorthite (Figs. 10, 12). We infer that the ^{16}O-poor compositions of anorthite in these CAIs resulted from postcrystallization isotopic exchange with an ^{16}O-poor reservoir. The oxygen isotopic composition of melilite in these CAIs is similar to that of anorthite, suggesting that melilite may have experienced isotopic exchange during the same process. The possible nature of this exchange is discussed below.

Postcrystallization oxygen isotopic exchange in the Allende Type C CAIs

Oxygen isotopic compositions of secondary monticellite (Δ^{17}O = –2‰), forsterite (Δ^{17}O = –5‰ to –3‰) and grossular (Δ^{17}O = –9‰) replacing lacy melilite in CAI *100* are not different outside analytical uncertainty from those of melilite (Δ^{17}O = –6‰), although grossular appears to be slightly ^{16}O-enriched (Table 1, Fig. 4). Since oxygen diffusion in forsterite is very slow (Ryerson et al., 1989), melilite+anorthite replaced by grossular+monticellite+forsterite must have been ^{16}O-depleted at the time of the replacement. The grossular-monticellite±forsterite intergrowths in CAI *160* measured with better precision by the CNRS/CRPG ion microprobe are ^{16}O-enriched relative to the massive and lacy melilite grains they replace (Fig. 2). Based on these

observations, we infer that oxygen isotopic exchange in melilite of *160* continued after formation of grossular-monticellite±forsterite intergrowths.

Thermodynamic analysis of the reactions which could have been involved in the formation of grossular (Hutcheon and Newton, 1981; Krot et al., 2007b):

(1) $3Ca_2MgSi_2O_7 + Ca_2Al_2SiO_7 + CaAl_2Si_2O_8 = 2Ca_3Al_2Si_3O_{12} + 3CaMgSiO_4$

(2) $3Ca_2MgSi_2O_7 + Ca_2Al_2SiO_7 + 2CaAl_2Si_2O_8 = 3Ca_3Al_2Si_3O_{12} + CaMgSiO_4 + Mg_2SiO_4$

(3) $4Ca_2MgSi_2O_7 + Ca_2Al_2SiO_7 + CaAl_2Si_2O_8 = 2Ca_3Al_2Si_3O_{12} + 4CaMgSiO_4 + CaSiO_3$

suggests that under equilibrium conditions for melilite of $Åk_{50-70}$ (covering nearly the entire range of melilite compositions in CAI *160*), replacement of melilite and anorthite by grossular, monticellite, ±forsterite, ±wollastonite occurred below ~750°C. The common presence of unaltered melilite-anorthite intergrowths in the Allende Type C CAIs *100*, *160* and *6-1-72* suggests lack of equilibrium. As a result, this reaction should only be used to constrain the upper temperature of grossular formation. Since grossular is not stable above this temperature, melting of the host CAI and associated oxygen isotopic exchange after formation of grossular can be excluded.

Either nebular or asteroidal heating could have resulted in the formation of grossular-bearing assemblages in Allende Type C CAIs (e.g., MacPherson, 2003; Fagan et al., 2005, 2006; Ushikubo et al., 2006; Krot et al., 2007b). We prefer an asteroidal setting for several reasons. (*i*) Pseudomorphic replacement of melilite and anorthite by grossular+monticellite±forsterite is a metamorphic reaction that requires a prolonged heating event, considering the large sizes (up to 25 μm) of grossular grains. This is difficult to reconcile with the short-duration heating events experienced by typical chondritic components in the solar nebula. At the same time, it is generally accepted that Allende experienced prolonged thermal metamorphism in an asteroidal setting at temperatures ≥350°C (e.g., Bonal et al., 2006 and references therein). (*ii*) Secondary grossular occurs also in the Allende and Mokoia chondrules, suggesting that both CAIs and chondrules experienced similar thermal processing (Kimura and Ikeda, 1998; Krot et al., 1998 and references therein). Haggerty and McMahon (1979), McMahon and Haggerty (1980) and Blum et al. (1989) reached similar conclusions based on observations of metal-magnetite-sulfide assemblages in Allende chondrules and CAIs. Neither CAIs nor chondrules in the reduced CV chondrites show evidence for secondary grossular; grossular is also absent in Kaba (Kimura and Ikeda, 1998) – aqueously altered oxidized CV chondrite of the Bali-like subgroup – which

experienced lower temperature thermal metamorphism than Allende (Bonal et al., 2006). (*iii*) The aluminum-magnesium systematics of most grossular grains (Hutcheon and Newton, 1981; MacPherson et al., 1995; Fagan et al., 2005, 2006) suggest late-stage formation, which is difficult to reconcile with prolonged nebular heating. We note, however, that both high ~$(1\text{-}3)\times10^{-5}$ and the low $(4.7\pm2.6)\times10^{-6}$ initial $^{26}Al/^{27}Al$ ratios have been recently inferred for several grossular-anorthite and grossular-melilite intergrowths from Allende CAIs (Fagan et al., 2005, 2006; Ushikubo et al., 2006). If the observed $^{26}Mg^*$ in grossular are not inherited from primary melilite and anorthite, multistage formation of grossular would be required. More work is needed to resolve this issue.

If grossular-monticellite±forsterite pseudomorphs formed during thermal metamorphism on the CV asteroid, at least some of the oxygen isotopic exchange of melilite and anorthite in Allende CAIs must have occurred in an asteroidal setting as well. Since oxygen isotopic exchange during anhydrous thermal metamorphism is probably sluggish, we suggest oxygen isotopic re-equilibration occurred during fluid-assisted metamorphism (Ash et al., 1999; Ash and Young, 2000; Jabeen et al., 1998a,b, 1999; Krot et al., 1998, 2006; Young et al., 1999; Zolotov et al., 2006). The oxygen isotopic composition of the fluid(s) operated on the CV parent asteroid ($\Delta^{17}O \sim -3‰$ to 0‰) can be inferred from the oxygen isotopic compositions of the Allende chondrules (e.g., Ash et al., 1999; Ash and Young, 2000; Jabeen et al., 1998a,b, 1999) or secondary minerals directly precipitated from aqueous/hydrothermal solutions, including fayalite, salite-hedenbergite pyroxenes, andradite and wollastonite, and magnetite that formed by oxidation of Fe,Ni-metal (Choi et al., 2000; Hua et al., 2005; Krot et al., 2006 and references therein; Fig. 14).

If our conclusion is correct, melilite and anorthite grains in many CAIs from the least metamorphosed CV chondrites are expected to be ^{16}O-enriched relative to the majority, ^{16}O-depleted melilite grains from Allende CAIs. This is supported by the common presence of ^{16}O-rich ($\Delta^{17}O$ up to –25‰) melilite in Type A CAIs from the CV3.1 Kaba (Nagashima et al., 2007).

Melilite in CAIs from metamorphosed CO chondrites is systematically ^{16}O-depleted relative to melilite from the primitive CO chondrites Y-81020 (CO3.0) and Colony (CO3.1) (Wasson et al., 2001; Itoh et al., 2004). The metamorphosed CO chondrites and Allende contain similar secondary minerals (Rubin, 1998), suggesting that the former also experienced fluid-assisted thermal metamorphism. We infer that the ^{16}O-depletion of melilite in metamorphosed CO

chondrites may also reflect isotopic exchange during fluid-assisted metamorphism. Experimental studies of oxygen isotopic exchange between water vapor and melilite are needed to test this hypothesis.

CONCLUSIONS

1. Spinel, massive and lacy Al,Ti-diopside in *100*, *160* and *CG5* are ^{16}O-rich ($\Delta^{17}O \leq -20‰$), suggesting that these CAIs were melted in an ^{16}O-rich nebular gas. Anorthite and melilite are ^{16}O-depleted ($\Delta^{17}O = -15‰$ to $-2‰$) relative to spinel and Al,Ti-diopside, indicating that anorthite and melilite experienced post-crystallization oxygen isotopic exchange with an ^{16}O-poor reservoir.

2. In *6-1-72*, lacy Al,Ti-diopside of the Type C portion and massive Al,Ti-diopside of the apparently relict Type B-like portion are similarly ^{16}O-depleted ($\Delta^{17}O \sim -13‰$) relative to spinel ($\Delta^{17}O = -23‰$), suggesting Al,Ti-diopside in both portions experienced melting events in an ^{16}O-depleted ($\Delta^{17}O \sim -13‰$) nebular gas, whereas spinel is relict. Anorthite and melilite are ^{16}O-depleted ($\Delta^{17}O = -9‰$ to $-2‰$) relative to spinel and Al,Ti-diopside, suggesting that anorthite and melilite experienced additional post-crystallization oxygen isotopic exchange with an ^{16}O-poor reservoir.

3. Spinel, Al,Ti-diopside, anorthite and melilite in CAIs *93*, *ABC* and in the mantle of *TS26* are ^{16}O-depleted ($\Delta^{17}O = -16‰$ to $-3‰$) compared to the uniformly ^{16}O-rich ($\Delta^{17}O \leq -20‰$) CAIs in primitive chondrites. Spinel in the core of *TS26* is ^{16}O-rich ($\Delta^{17}O = -20‰$), whereas Al,Ti-diopside grains are ^{16}O-depleted ($\Delta^{17}O = -15‰$ to $-10‰$). Anorthite and melilite of *ABC*, *93* and *TS26* are ^{16}O-depleted ($\Delta^{17}O = -5‰$ and $-1‰$) relative to spinel and Al,Ti-diopside. We conclude that spinel, anorthite, Al,Ti-diopside, and melilite of *93* and *ABC* and Al,Ti-diopside in the mantle of *TS26* experienced oxygen isotopic exchange during re-melting in the presence of an ^{16}O-poor ($\Delta^{17}O \geq -10‰$) nebular gas in the chondrule-forming region(s). Spinel in the core of *TS26* is relict, whereas Al,Ti-diopside experienced melting and oxygen isotopic exchange in an ^{16}O-depleted nebular gas. This melting event may have occurred contemporaneously or preceded the melting episode that produced the finer-grained and more ^{16}O-depleted Al,Ti-diopside mantle.

Subsequently, anorthite and melilite experienced additional, post-crystallization oxygen isotopic exchange.

4. Grossular-monticellite intergrowths in CAI *160* are ^{16}O-enriched relative to the melilite+anorthite they replace. Because pseudomorphic replacement of lacy melilite by grossular and monticellite occurred during thermal metamorphism at temperatures below 750°C, oxygen isotopic exchange of melilite and anorthite in Type C CAIs must have continued after formation of grossular. We suggest that at least some of oxygen isotopic exchange in melilite and anorthite in Allende CAIs occurred during fluid-assisted thermal metamorphism. Similar processes may have also affected melilite and anorthite in CAIs from metamorphosed CO chondrites. Experimental studies of oxygen isotopic exchange between water vapor and melilite are needed to test this hypothesis.

Acknowledgements: This work was supported by NASA grants NAG5-10610 (A. N. Krot, P.I.), NAG5-11591 (K. Keil, P.I.), NAG5-10468 (G. J. MacPherson, P.I.), and NNH04AB471 (I.D. Hutcheon, P.I.) and Monkasho grants (H. Yurimoto, P.I.). We thank L. Grossman for providing sample of CAI *6-1-72*. We thank Drs. M. Cosarinsky, M. Kimura, R. Ash and S. Russell (AE) for detailed reviews and suggestions which helped to focus the paper. We thank S. Russell for her patience in handling this manuscript. This work was performed under the auspices of the U. S. Department Energy by the University of California, Lawrence Livermore National Laboratory under Contract No. W-7405-Eng-48. This is School of Ocean and Earth Science and Technology publications number XXXX and Hawai‘i Institute of Geophysics and Planetology publication number XXXX. Prepared in part by LLNL under Contract DE-AC52-07NA27344

REFERENCES

Aléon J., Krot A. N., and McKeegan K. D. (2002) Ca-Al-rich inclusions and amoeboid olivine aggregates from the CR carbonaceous chondrites. *Meteorit. Planet. Sci.* **37**, 1729-1755.

Aléon J., Krot A. N., McKeegan K. D., MacPherson G. J., and Ulyanov A. A. (2005a) Fine-grained, spinel-rich inclusions from the reduced CV chondrite Efremovka: II. Oxygen isotopic compositions. *Meteorit. Planet. Sci.* **40**, 1043-1058.

Aléon J., El Goresy A., and Zinner E. (2005b) First evidence for co-existing ^{16}O-poor and ^{16}O-rich gases in the early solar nebula inferred from a compound Ca-Al-rich inclusion from

Efremovka (abstract). In Workshop on *Oxygen in the Earliest Solar System*, Gatlinburg, Tennessee, LPI Contribution No. 1278, 8.

Amelin Y., Krot A. N., Hutcheon I. D., and Ulyanov A. A. (2002) Pb isotopic ages of chondrules and Ca,Al-rich inclusions. *Science* **297**, 1678-1683.

Ash R. D., Young E. D., Rumble III D., Alexander C. M. O'D., and MacPherson G. J. (1999) Oxygen isotope systematics in Allende chondrules (abstract). *Lunar Planet. Sci.* **XXX**, #1836.

Ash R. D. and Young E. D. (2000) Clarity and confusion: The history of Allende chondrules as evinced by oxygen isotopes (abstract). *Lunar Planet. Sci.* **XXX**, #1881.

Blum J. D., Wasserburg G. J., Hutcheon I. D., Beckett J. R., and Stolper E. M. (1989) Origin of opaque assemblages in CV3 meteorites: implications for nebular and planetary processes, *Geochim. Cosmochim Acta* **53**, 543-556.

Bonal L., Quirico E., Bourot-Denise M., and Montagnac G. (2006) Determination of the petrologic type of CV3 chondrites by Raman spectroscopy of included organic matter. *Geochim. Cosmochim. Acta* **70**, 1849-1863.

Choi B.-G., Krot A. N., and Wasson J. T. (2000) Oxygen-isotopes in magnetite and fayalite in CV chondrites Kaba and Mokoia. *Meteorit. Planet. Sci.* **35**, 1239-1248.

Clayton R. N., Onuma N., Grossman L., and Mayeda T. K. (1977) Distribution of the pre-solar component in Allende and other carbonaceous chondrites. *Earth Planet. Sci. Lett.* **304**, 209-224.

Cosarinsky M., Leshin L. A., MacPherson G. J., Krot A. N., and Guan Y. (2002) Oxygen isotopic composition of olivines from matrices and accretionary rims around Ca-Al-rich inclusions in CV chondrites (abstract). *Meteorit. Planet. Sci.* **37 (suppl.),** A38.

Cosarinsky M., Leshin L. A., MacPherson G. J., Krot A. N., and Guan Y. (2003) Oxygen isotope composition of Ca-Fe-rich silicates in and around al Allende Ca-Al-rich inclusion (abstract). *Lunar Planet. Sci.* **XXXIV**, #1043.

Fagan T. J., Krot A. N., Keil K., and Yurimoto H. (2004) Nebular setting of oxygen isotopic alteration in a coarse-grained Ca-Al-rich inclusion from Efremovka. *Meteorit. Planet. Sci.* **39**, 1257-1272.

Fagan T. J., Guan Y., MacPherson G. J., and Huss G. R. (2005) Al-Mg isotopic evidence for separate nebular and parent body alteration events in two Allende CAIs (abstract). *Lunar Planet. Sci.* **XXXVI**, #1820.

Fagan T. J., Guan Y., and MacPherson G. J. (2006) Al-Mg isotopic constraints on alteration of Allende Ca-Al-rich inclusions (abstract). *Lunar Planet. Sci.* **XXXVII**, #1213.

Fagan T. J., Krot A. N., Kobayashi S., and Yurimoto H. (2007) Correlation between texture and oxygen isotopic systematics in CAIs from Acfer 094 (abstract). *Lunar Planet Sci*. **XXXVIII**, #1252.

Greenwood J. P. (2004) Disequilibrium melting of refractory inclusions: A mechanism for high-temperature oxygen isotope exchange in the solar nebula (abstract). *Lunar Planet. Sci.* **XXXV**, #2132.

Gurenko A. A. and Chaussidon M. (2002) Oxygen isotopic variations in primitive tholeiites of Iceland: evidence from a SIMS study of glass inclusions, olivine phenocrysts and pillow rim glasses. *Earth Planet. Sci. Lett.* **205**, 63-79.

Haggerty S. E. and McMahon B. M. (1979) Magnetite-sulfide-metal complexes in the Allende meteorite, *Proc. Lunar Planet. Sci 10th*, 851-870.

Harazono K. and Yurimoto H. (2003) Oxygen isotopic variations in a fluffy Type A CAI from the Vigarano meteorite (abstract). *Lunar Planet. Sci.* **XXXIV**, #1540.

Hua X., Huss G. R., Tachibana S., and Sharp T. G. (2005) Oxygen, silicon, and Mn-Cr isotopes of fayalite in the Kaba oxidized CV3 chondrite: Constraints for its formation history. *Geochim. Cosmochim. Acta* **69**, 1333-1348.

Hutcheon I. D. and Newton R. C. (1981) Mg isotopes, mineralogy, and mode of formation of secondary phases in C3 refractory inclusions (abstract). *Lunar. Planet. Sci.* **XII**, 491-493.

Imai H. and Yurimoto H. (2000) Oxygen and magnesium isotopic distributions in a Type C CAI from the Allende meteorite (abstract). *Lunar Planet. Sci.* **XXXI**, #1510.

Itoh S. and Yurimoto H. (2003) Contemporaneous formation of chondrules and refractory inclusions in the early Solar System. *Nature* **423**, 728-731.

Itoh S., Kojima H., and Yurimoto H. (2004) Petrography and oxygen isotopic compositions in refractory inclusions from CO chondrites. *Geochim. Cosmochim. Acta* **68**, 183-194.

Ito M., Nagasawa H., and Yurimoto H. (2004) Oxygen isotopic SIMS analysis in Allende CAI: Details of the very early thermal history of the solar system. *Geochim. Cosmochim. Acta* **68**, 2905-2923.

Jabeen I., Kusakabe M., Nakamura T., and Nagao K. (1998a) Oxygen isotopic signature in Allende chondrules (abstract). *Meteorit. Planet. Sci.* **33** (Suppl.), A76-A77.

Jabeen I., Kusakabe M., Nakamura T., and Nagao K. (1998b) Oxygen isotope study of Tsukuba chondrite, some HED meteorites and Allende chondrules. *Antarct. Meteorite Res.* **11**, 122-135.

Jabeen I., Kusakabe M., Nakamura T., and Nagao K. (1999) Parent body processes in Allende: Evidence from oxygen isotope study of the Allende chondrules (abstract). *Symp. Antarct. Meteorit.* **24**, 59-61.

Kim G. L., Yurimoto H., and Sueno S. (2002) Oxygen isotopic composition of a compound Ca-Al-rich inclusion from Allende meteorite: Implications for origin of palisade bodies and O-isotopic environment in the CAI-forming region. *J. Mineral. Petrol. Sci.* **97**, 161-167.

Kimura M. and Ikeda Y. (1998) Hydrous and anhydrous alterations of chondrules in Kaba and Mokoia CV chondrites. *Meteorit. Planet. Sci.* **33**, 1139-1146.

Kita N. T., Ushikubo T., Fu B., Spicuzza M. J., and Valley J. W. (2007) Analytical Developments on oxygen three isotope analyses using a new generation ion microprobe IMS-1280 (abstract). *Lunar Planet. Sci.* **XXXVIII**, #1981.

Krot A. N., Petaev M. I., Scott E. R. D., Choi B.-G., Zolensky M. E., and Keil K. (1998) Progressive alteration in CV3 chondrites: More evidence for asteroidal alteration. *Meteorit. Planet. Sci.* **33**, 1065-1085.

Krot A. N., Ulyanov A. A., Meibom A., and Keil K. (2001) Forsterite-rich accretionary rims around Ca, Al-rich inclusions from the reduced CV3 chondrite Efremovka. *Meteorit. Planet. Sci.* **36**, 611-628.

Krot A. N., McKeegan K. D., Leshin L. A., MacPherson G. J., and Scott E. R. D. (2002) Existence of an ^{16}O-rich gaseous reservoir in the solar nebula. *Science* **295**, 1051-1054.

Krot A. N., Hutcheon I. D., Yurimoto H., Cuzzi J. N., McKeegan K. D., Scott E. R. D., Libourel G., Chaussidon M., Aléon J., and Petaev M. I. (2005a) Evolution of oxygen isotopic composition in the inner solar nebula. *Astrophys. J.* **622**, 1333-1342.

Krot A. N., Yurimoto H., Hutcheon I. D., and MacPherson G. J. (2005b) Relative chronology of CAI and chondrule formation: Evidence from chondrule-bearing igneous CAIs. *Nature* **434**, 998-1001.

Krot A. N., Hutcheon I. D., Brearley A. J., Pravdivtseva O. V., Petaev M. I., and Hohenberg C. M. (2006) Timescales for secondary alteration of chondritic meteorites. In *Meteorites and The Early Solar System II*, eds. Lauretta D. and McSween H. Y., Jr., pp. 525-553.

Krot A. N., Yurimoto H., Hutcheon I. D., MacPherson G. J., and Paque J. (2007a) Remelting of refractory inclusions in the chondrule-forming regions: Evidence from the chondrule-bearing Type C calcium-aluminum-rich inclusions from Allende. *Meteorit. Planet. Sci.*, in press.

Krot A. N., Yurimoto H., Hutcheon I. D., Libourel G., Chaussidon M., Petaev M. I., MacPherson G. J., Paque-Heather J., and Wark D. (2007b) Type C CAIs from Allende: Evidence for multistage formation. *Geochim. Cosmochim. Acta*, in press.

MacPherson G. J. (2003) Calcium-aluminum-rich inclusions in chondritic meteorites. In Meteorites, Comets, and Planets, ed. Davis A. M., Vol. 1, Treatise on Geochemistry, eds. Holland D. D. and Turekian K. K. (Oxford: Elsevier-Pergamon), 201-247.

MacPherson G. J.., Wark D. A., and Armstrong J. T. (1988) Primitive material surviving in chondrites: Refractory inclusions. In *Meteorites and the Early Solar System* (J. F. Kerridge and M. S. Matthews, eds.), pp. 746-807. Univ. of Arizona Press, Tucson.

MacPherson G. J., Davis A. M., and Zinner E. K. (1995) The distribution of aluminum-26 in the early solar system: A reappraisal. *Meteoritics* **30**, 365-386.

McKeegan K. D., Leshin L. A., and MacPherson G. J. (1998) Oxygen isotopic stratigraphy in a Vigarano type-A calcium-aluminum-rich inclusion (abstract). *Meteorit. Planet. Sci.* **33 (Suppl.)**, A102-A103.

McMahon B. M. and Haggerty S. E. (1980) experimental studies bearing on the magnetite-alloy-sulfide association in the Allende meteorite: constraints on the conditions of chondrule formation, *Proc. Lunar Planet. Sci Conf. 11th*, 1003-1025.

Nagashima K., Krot A. N., Huss G. R., and X. Hua (2007) Common presence of ^{16}O-rich melilite in calcium-aluminum-rich inclusions from the least metamorphosed CV carbonaceous chondrite Kaba (abstract). *Lunar Planet Sci.* **XXXVIII**, #2059.

Petaev M. I. and Wood J. A. (2005) Meteoritic constraints on temperatures, pressures, cooling rates, chemical compositions, and modes of condensation in the solar nebula. in *Chondrites and the Protoplanetary Disk*, eds. Krot A. N., Scott E. R. D. and Reipurth B. Astronomical Society of the Pacific Conference Series **341**, pp. 373-407.

Pouchou J. L. and Pichoir F. (1984) A new model for quantitative X-ray microanalysis. I Application to the analysis of homogeneous samples. *La Recherche Aerospatiale*, 3, 13-38.

Rubin A. E. (1998) Correlated petrologic and geochemical characteristics of CO3 chondrites. *Meteorit. Planet. Sci.* **33**, 385-391.

Ryerson F. J., Durham W. B., Cherniak D. J., and Lanford W.A. (1989) Oxygen diffusion in olivine: Effect of oxygen fugacity and implication for creep. *J. Geophys. Res.* **94**, 4105-4118.

Ryerson F. J. and McKeegan K. D. (1994) Determination of oxygen self-diffusion in akermanite, anorthite, diopside, and spinel: Implications for oxygen isotopic anomalies and the thermal histories of Ca-Al-rich inclusions. *Geochim. Cosmochim. Acta* **58**, 3713-3734.

Scott E. R. D. and Krot A. N. (2003) Chondrites and their components. In *Meteorites, Comets and Planets* (ed. A.M. Davis) Vol. 1, *Treatise on Geochemistry* (eds. H.D. Holland and K.K. Turekian), pp. 143-200. Elsevier, Oxford.

Stolper E. (1982) Crystallization sequences of Ca-Al-rich inclusions from Allende: an experimental study. *Geochim. Cosmochim. Acta* **46**, 2159-2180.

Stolper E. and Paque J. M. (1986) Crystallization sequences of Ca-Al-rich inclusions from Allende: The effects of cooling rate and maximum temperature. *Geochim. Cosmochim. Acta* **50**, 1785-1806.

Thrane K., Bizzarro M., and Baker J. A. (2006) Extremely brief formation interval for refractory inclusions and uniform distribution of ^{26}Al in the early Solar System. *Astrophys. J.* **646**, L159-L162.

Ushikubo T., Guan Y., Hiyagon H., Sugiura N., and Leshin L. A. (2006) ^{36}Cl, ^{26}Al and oxygen isotopes in an Allende CAI: Implications for secondary alteration in the early solar system (abstract). *Lunar Planet. Sci.* **XXXVII**, #2082.

Wark D. A. (1987) Plagioclase-rich inclusions in carbonaceous chondrite meteorites: Liquid condensates? *Geochim. Cosmochim. Acta* **51**, 221-242.

Wasson J. T., Yurimoto H., and Russell S. S. (2001) ^{16}O-rich melilite in CO3.0 chondrites. Possible formation of common, ^{16}O-poor melilite by aqueous alteration. *Geochim. Cosmochim. Acta* **65**, 4539-4549.

Yoshitake M., Koide Y., and Yurimoto H. (2002) Distributions of oxygen isotopes in Wark-Lovering rim of a Type B2 CAI from the Vigarano meteorite (abstract). *Lunar Planet. Sci.* **XXXIII**, #1502.

Young E. D., Ash R. D., England P., and Rumble D. (1999) Fluid flow in chondritic parent bodies: Deciphering the compositions of planetesimals. *Science* **286**, 1331-1335.

Yurimoto H., Morioka M., and Nagasawa H. (1989) Diffusion in single-crystals of melilite: I. Oxygen. *Geochim. Cosmochim. Acta* **53**, 2387-2394.

Yurimoto H., Ito M., and Nagasawa H. (1998) Oxygen isotope exchange between refractory inclusion in Allende and solar nebula gas. *Science* **282**, 1874-1877.

Zolotov M. Y., Mironenko M. V., and Shock E. L. (2006) Thermodynamic constraints on fayalite formation on parent bodies of chondrites. *Meteorit. Planet. Sci.* **41**, 1775-1797.

Fig. 1. Backscattered electron (BSE) images of a Type C CAI *160*. Ion probe spots are numbered; numbers correspond to those listed in Table 1. an = anorthite; di = Al,Ti-diopside; grs = grossular; mel = melilite; mnl = monticellite; sp = spinel.

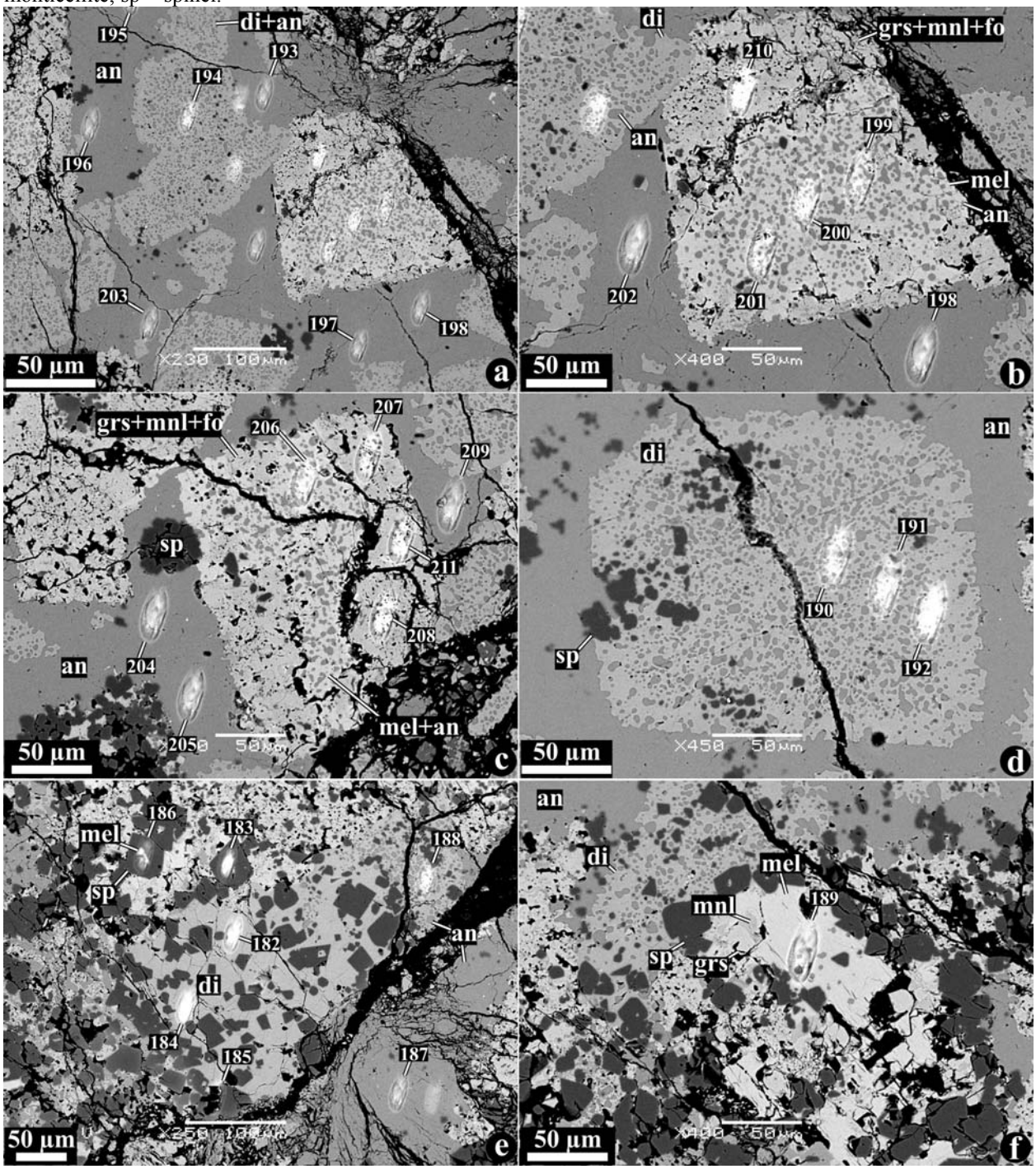

Fig. 2. Oxygen isotopic compositions of a Type C CAI *160*. In "a", data are plotted as $\delta^{17}O$ *vs.* $\delta^{18}O$; to illustrate variations in oxygen isotopic compositions of different minerals, in "b", the same data, grouped by minerals, are plotted as deviations from the terrestrial fractionation line (TFL), $\Delta^{17}O$ (= $\delta^{17}O - 0.52\times\delta^{18}O$). Carbonaceous chondrite anhydrous mineral (CCAM) line and TFL are shown for reference. an = anorthite; di = Al,Ti-diopside; grs+mnl = grossular + monticellite; mel = melilite; sp = spinel.

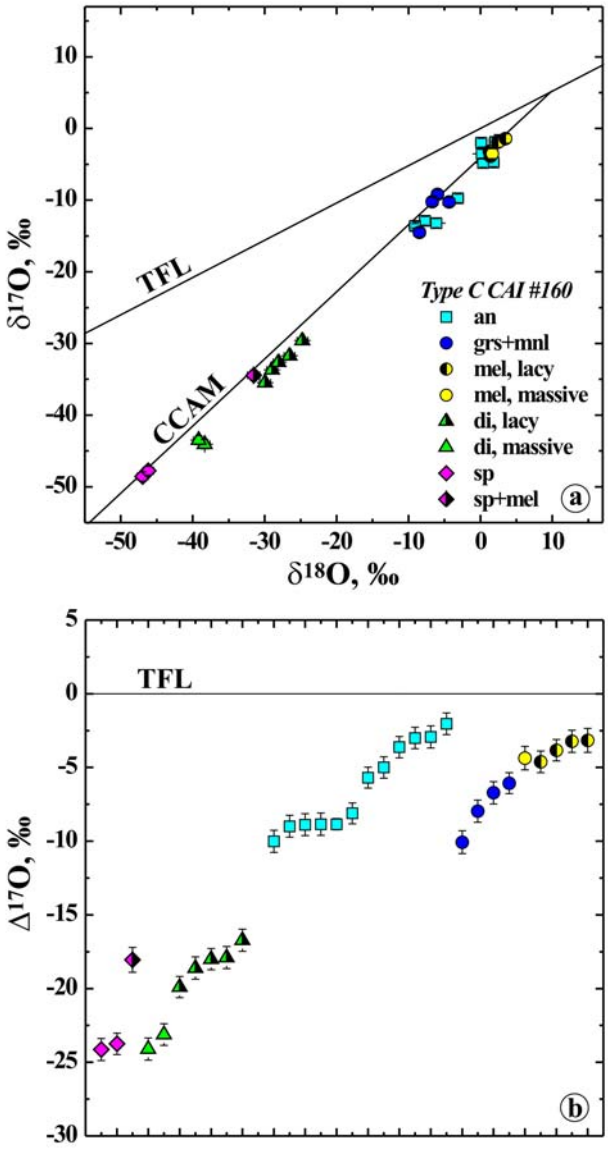

Fig. 3. BSE images of a Type C CAI *100*. Ion probe spots are outlined and numbered; numbers correspond to those listed in Table 1. an = anorthite; di = Al,Ti-diopside; fo = forsterite; grs = grossular; mel = melilite; mnl = monticellite; sp = spinel.

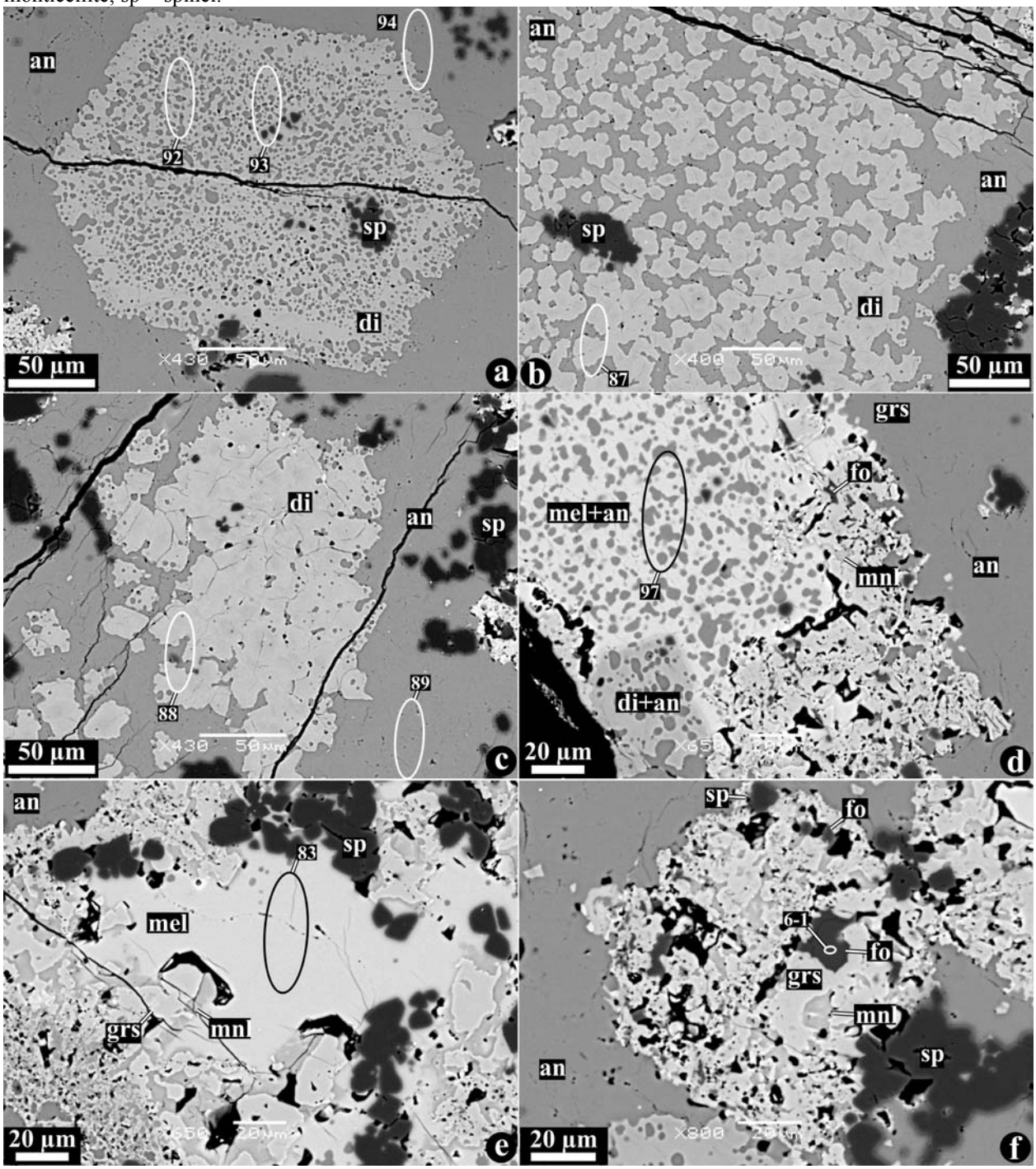

Fig. 4. Oxygen isotopic compositions of a Type C CAI *100* collected using CNRS-CRPG (a, b; 2σ error) and HU (c, d; 1σ error) ion microprobes. In "a" and "b", data are plotted as $\delta^{17}O$ *vs.* $\delta^{18}O$; in "c" and "d", the same data, grouped by minerals, are plotted as $\Delta^{17}O$. an = anorthite; di = Al,Ti-diopside; fo = forsterite; grs = grossular; mel = melilite; mnl = monticellite; sp = spinel.

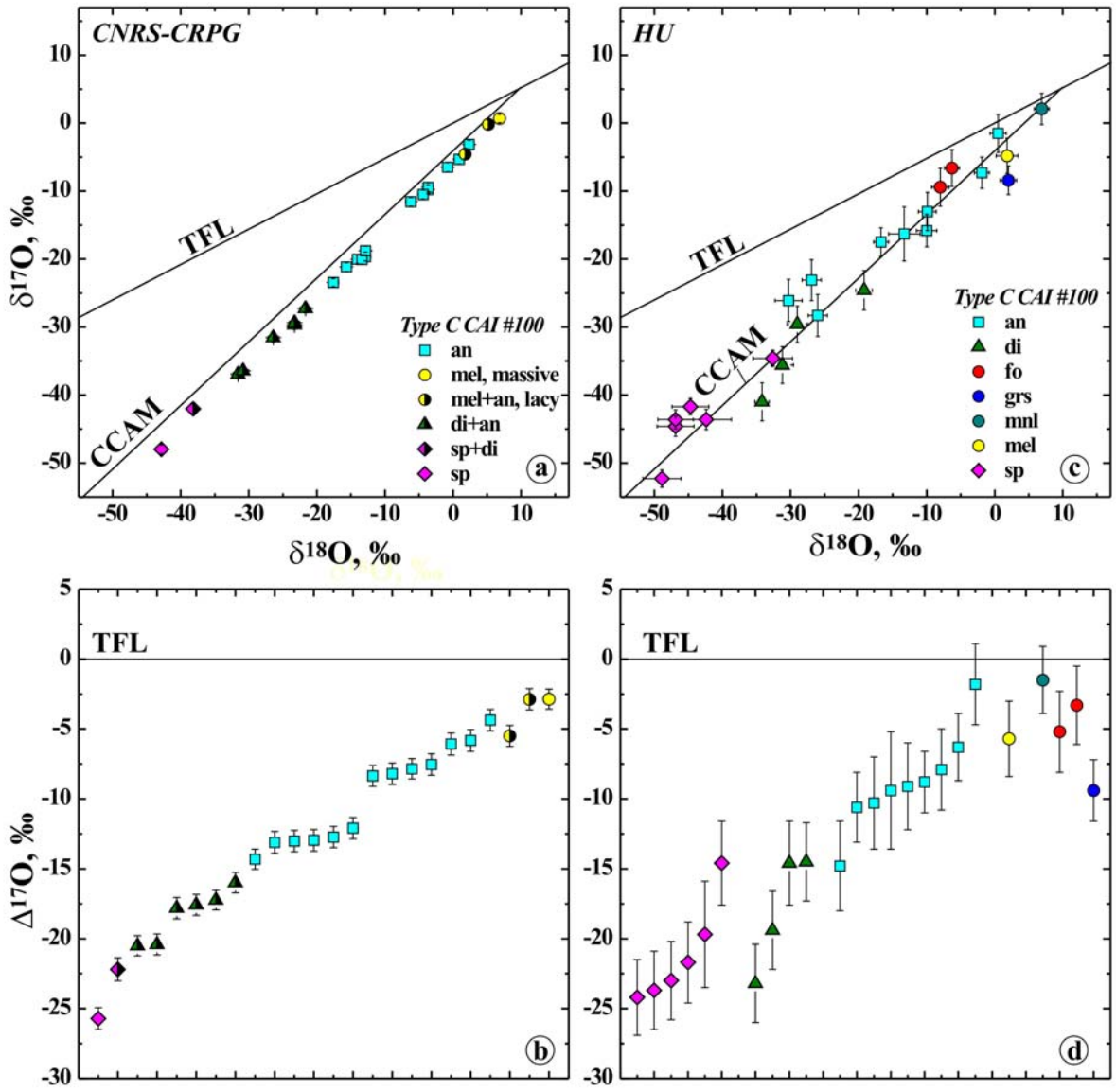

Fig. 5. BSE of the Type C (a-c) and Type B-like (d-f) portions of a CAI *6-1-72*. Ion probe spots are outlined and numbered; numbers correspond to those listed in Table 1. Ellipsoid spots are from CNRS/CRPG ims-1270; square regions are from UH ims-1280. an = anorthite; di = Al,Ti-diopside; fo = forsterite; grs = grossular; mel = melilite; mnl = monticellite; sp = spinel.

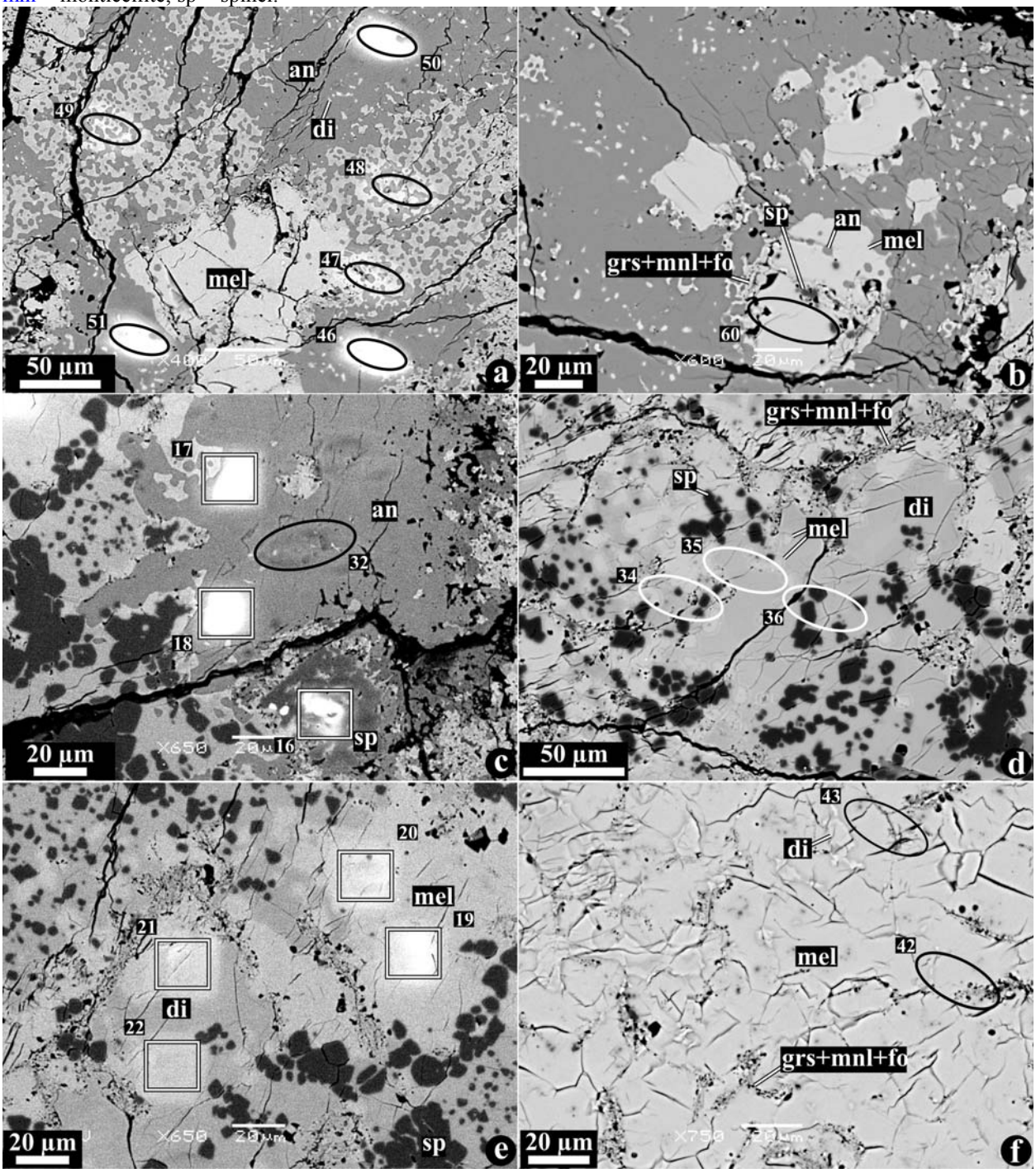

Fig. 6. Oxygen isotopic compositions of a the Type B-like and Type C portions of a CAI *6-1-72*. In "a", data are plotted as $\delta^{17}O$ *vs.* $\delta^{18}O$; to illustrate variations in oxygen isotopic compositions of different minerals, in "b", the same data, grouped by minerals, are plotted as $\Delta^{17}O$. an = anorthite; di = Al,Ti-diopside; grs = grossular; mel = melilite; sp = spinel. Legends in the top left corner and the bottom right corner correspond to data collected with the CNRS/CRPG and UH ion microprobes, respectively.

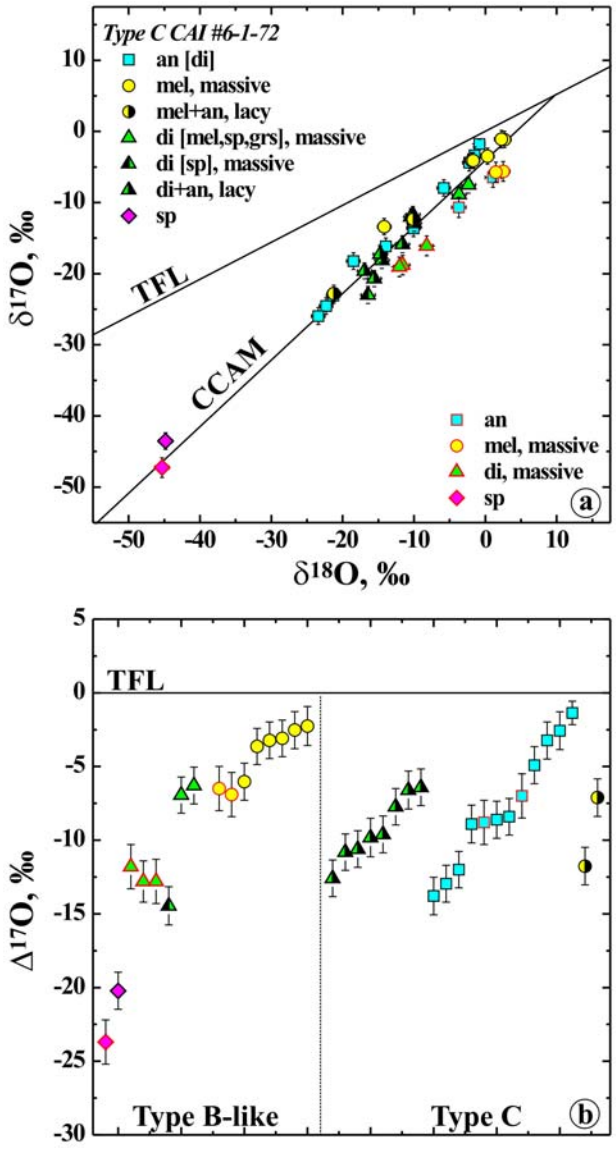

Fig. 7. BSE images of a Type C CAI *CG5*. Ion probe spots are outlined and numbered; numbers correspond to those listed in Table 1. an = anorthite; di = Al,Ti-diopside; mel = melilite; sp = spinel.

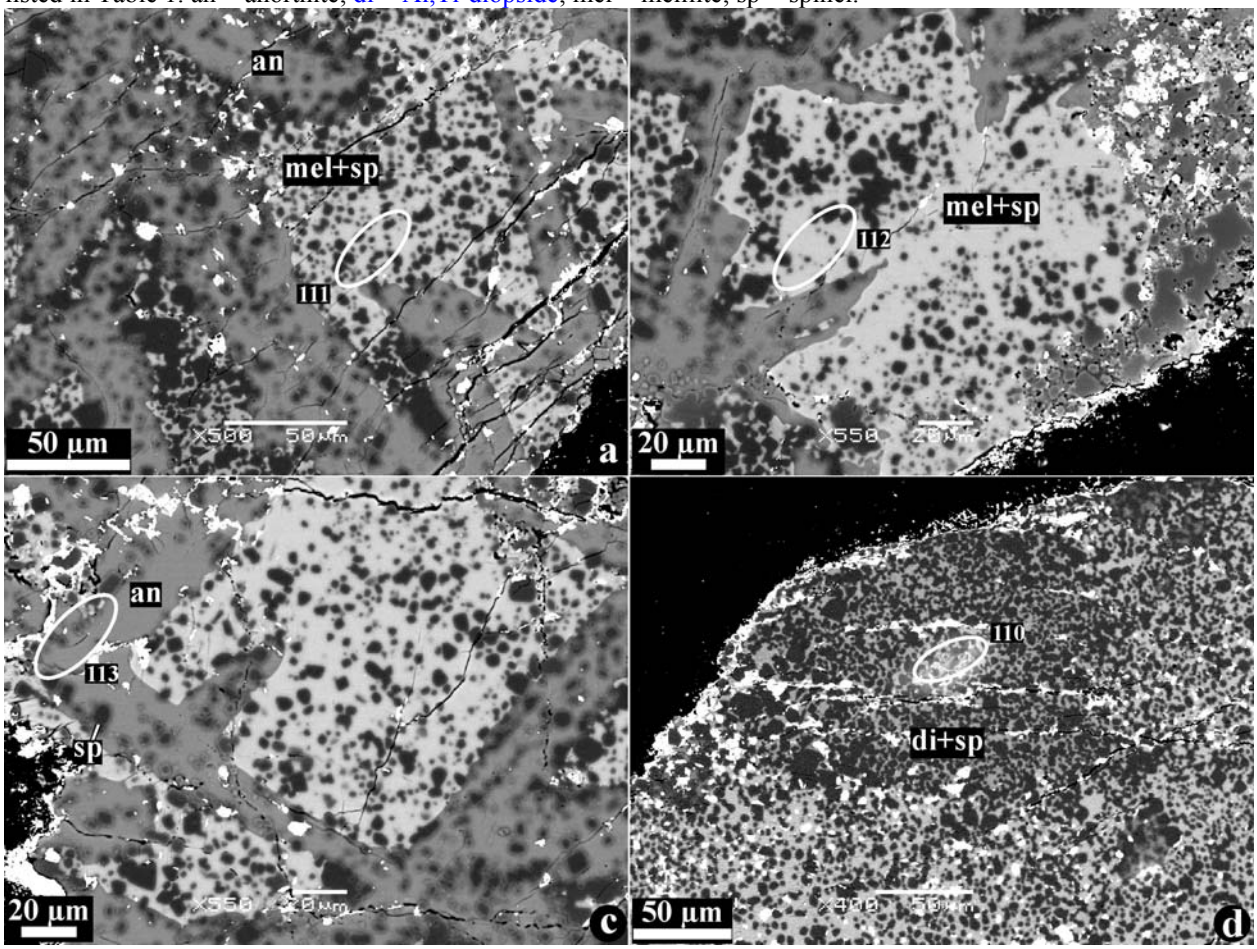

Fig. 8. Oxygen isotopic compositions of a Type C CAI *CG5*. In "a", data are plotted as $\delta^{17}O$ *vs.* $\delta^{18}O$; in "b", the same data are plotted as $\Delta^{17}O$. an = anorthite; di = Al,Ti-diopside; mel = melilite; sp = spinel.

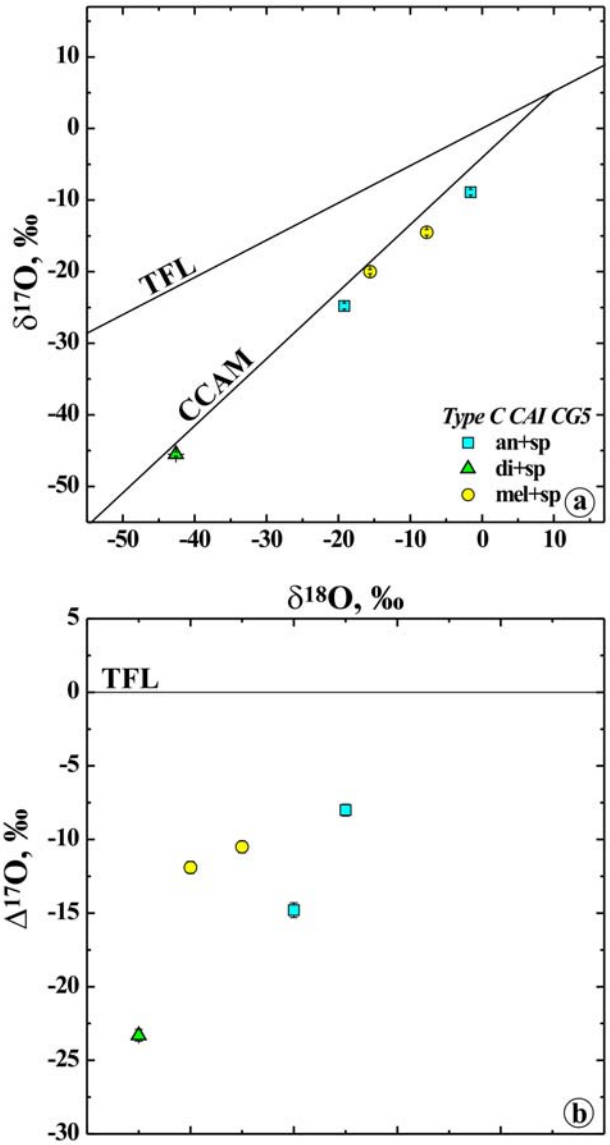

Fig. 9. (a) Combined elemental maps in Mg (red), Ca (green) and Al (blue) Kα X-rays, (b) combined elemental maps in Mg (red), Ti (green) and Al (blue) Kα X-rays, and (c-f) BSE images of a Type C *93*. Regions outlined in and labeled "a" are shown in detail in "c", "d", and "f". Region outlined in "d" is shown in detail in "e". Ion probe spots are outlined and numbered; numbers correspond to those listed in Table 1. an = anorthite; aug = augite; di = Al,Ti-diopside, fa = ferrous olivine; grs = grossular; mel = melilite; mnl = monticelllite; pg = pigeonite; sod = sodalite.

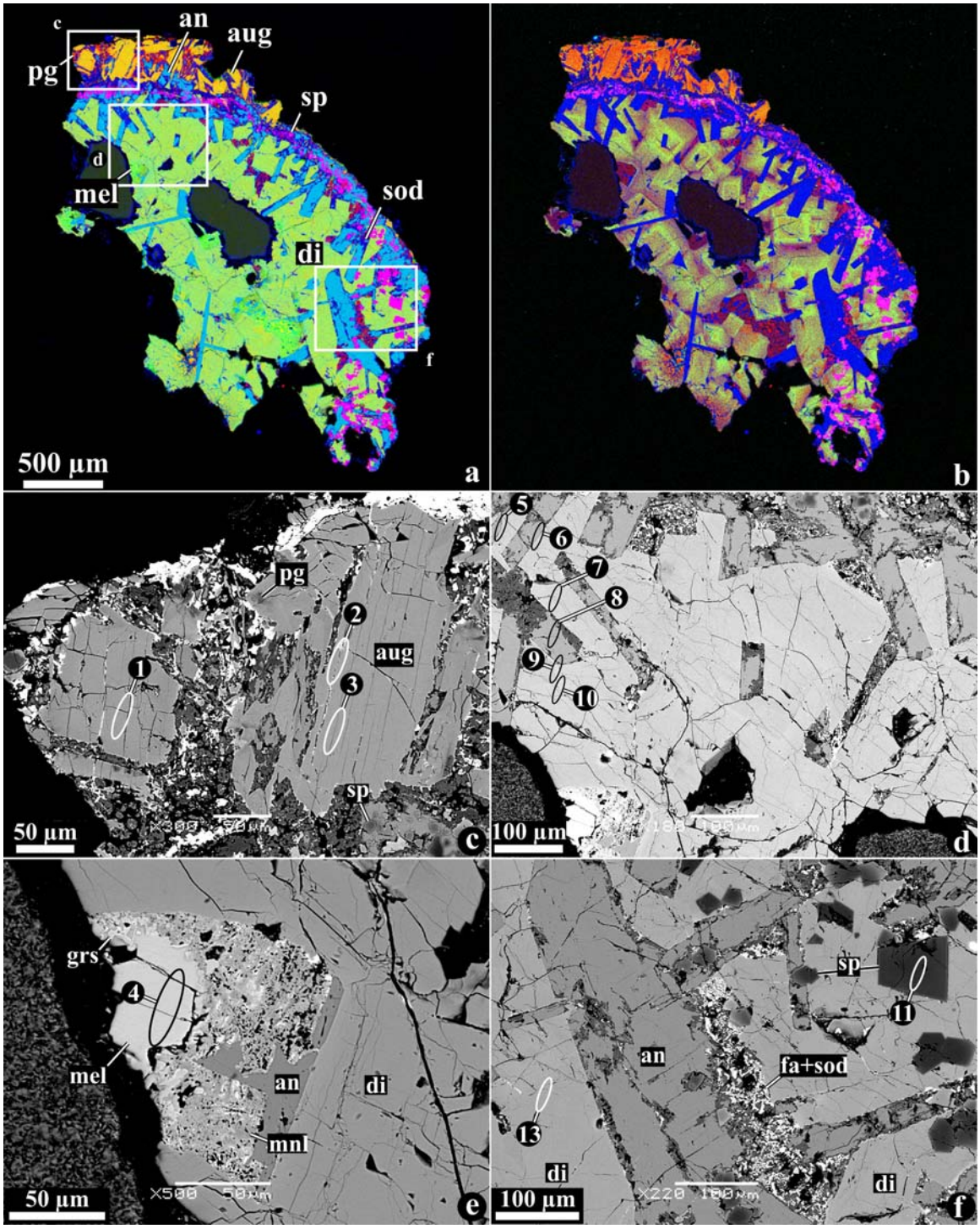

Fig. 10. Oxygen isotopic compositions of a Type C CAI *#93* with a chondrule-like, igneous rim. In "a", data are plotted as $\delta^{17}O$ *vs.* $\delta^{18}O$; in "b", the same data, grouped by minerals, are plotted as $\Delta^{17}O$. an = anorthite; aug = augite; di = Al,Ti-diopside; mel = melilite; sec = secondary minerals; sp = spinel.

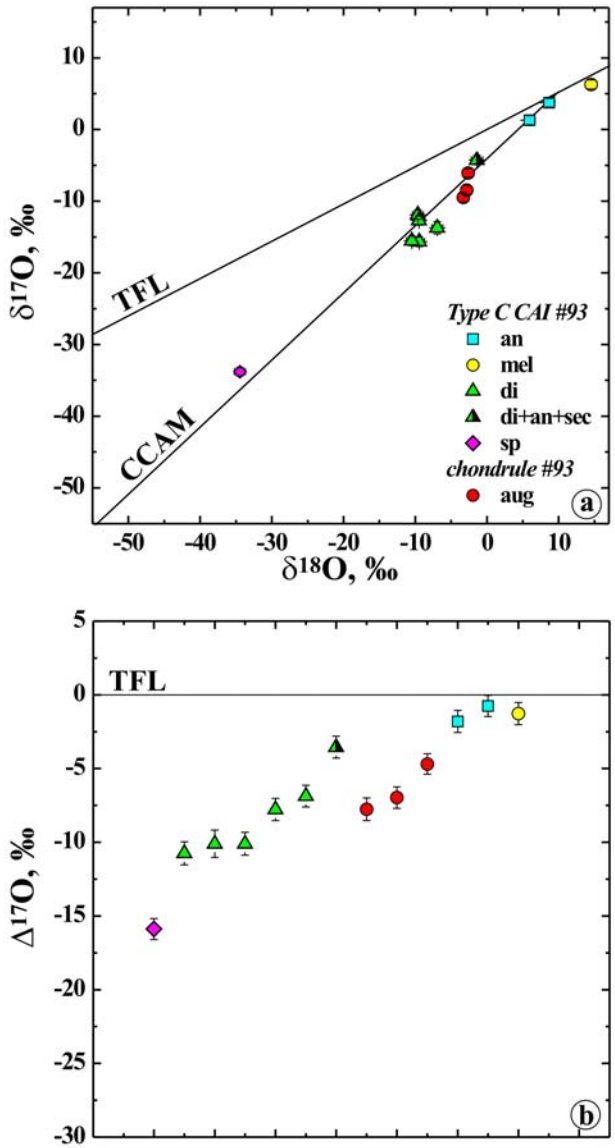

Fig. 11. (a) Combined elemental maps in Mg (red), Ca (green) and Al (blue) Kα X-rays, (b) combined elemental maps in Mg (red), Ti (green) and Al (blue) Kα X-rays, and (c-f) BSE images of a Type C *ABC*. Regions outlined in and labeled "b" are shown in detail in "c-f". Ion probe spots are outlined and numbered; numbers correspond to those listed in Table 1. an = anorthite; aug = augite; Cr-sp = chromium spinel; di = Al,Ti-diopside, fa = ferrous olivine; grs = grossular; lpx = low-Ca pyroxene; mel = melilite; mes = mesostasis; mnl = monticellite; nph = nepheline; pl = anorthitic plagioclase; sf = sulfide; sod = sodalite; sp = spinel; wol = wollastonite.

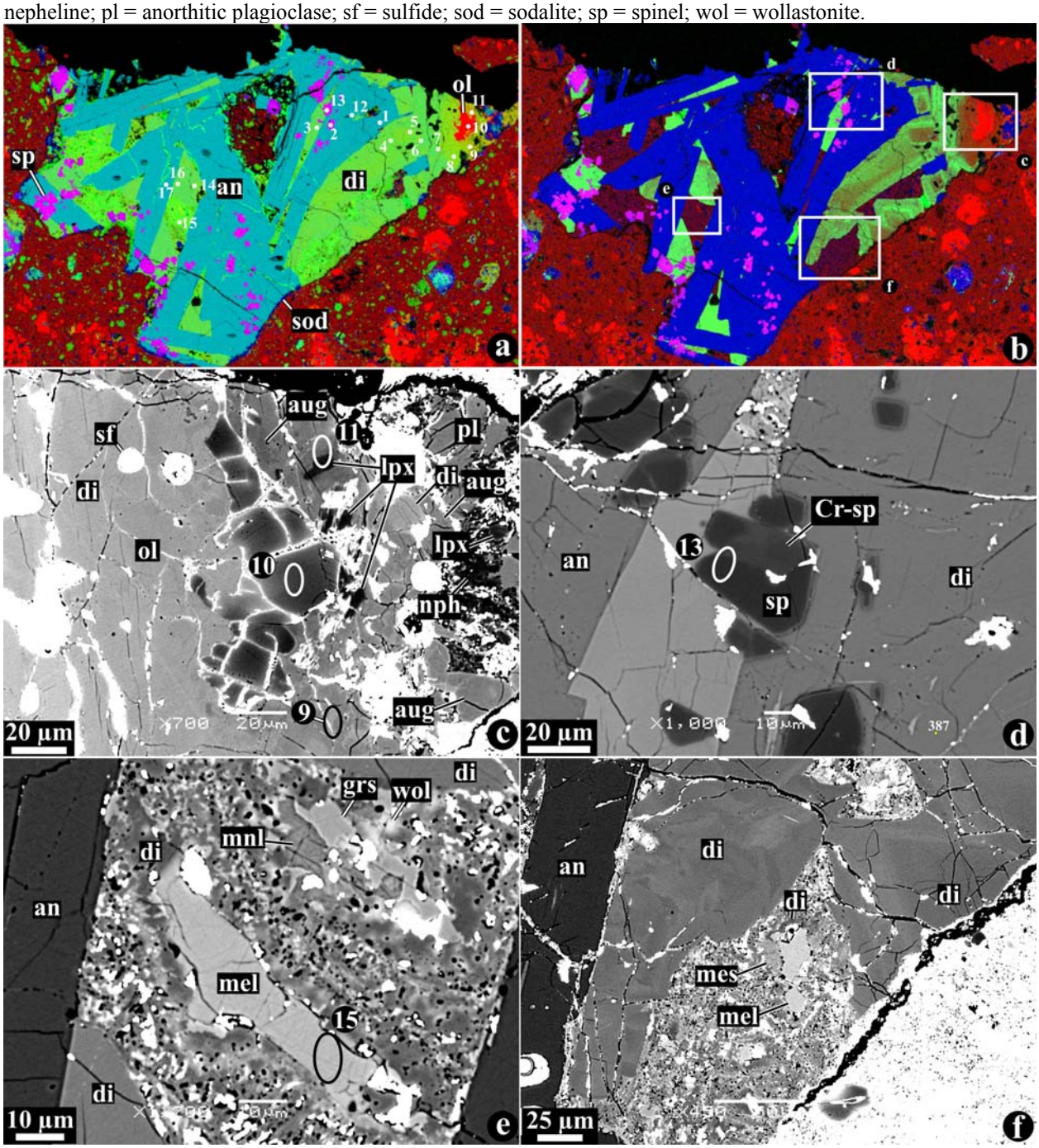

Fig. 12. Oxygen isotopic compositions of Type C CAIs *ABC* (a, b) and *TS26* (c, d) with chondrule fragments in their peripheries (from Krot et al., 2007b). In "a" and "c", data as plotted as $\delta^{17}O$ *vs.* $\delta^{18}O$; in "b" and "d", the same data, grouped by minerals, are plotted as $\Delta^{17}O$. an = anorthite; aug = augite; Cr-sp = Cr-spinel; di = Al,Ti-diopside; lpx = low-Ca pyroxene; mel = melilite; ol = olivine; sp = spinel.

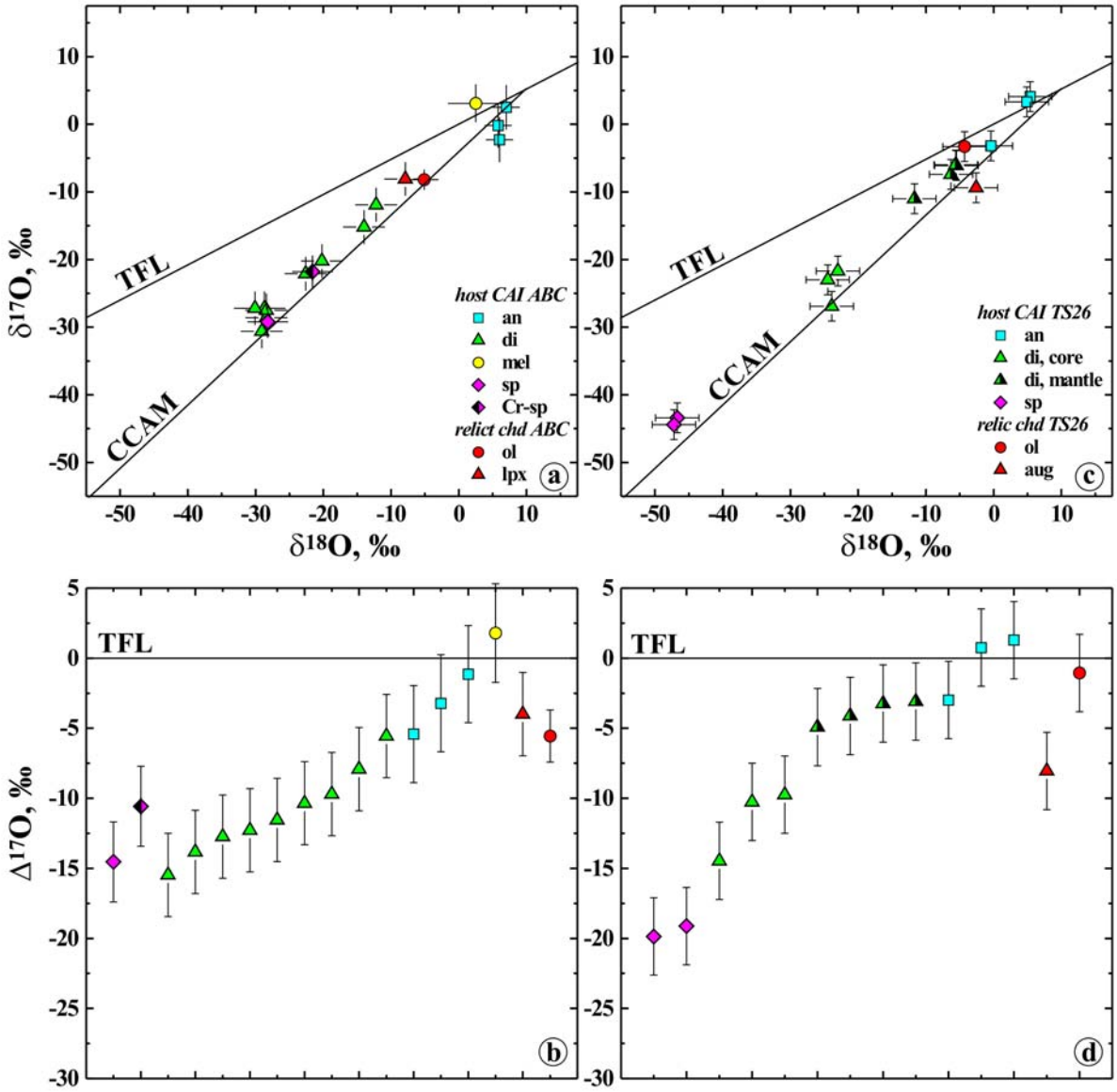

Fig. 13. Combined elemental maps in Mg (red), Ca (green) and Al (blue) Kα X-rays, (b) combined elemental maps in Mg (red), Ti (green) and Al (blue) Kα X-rays, and (c, d) BSE images of a Type C *TS26*. Regions outlined in and labeled "a" are shown in detail in "c" and "d". Ion probe spots are outlined and numbered; numbers correspond to those listed in Table 1. an = anorthite; aug = augite; di = Al,Ti-diopside; fa = ferrous olivine; lpx = low-Ca pyroxene; mel = melilite; sod = sodalite; sp = spinel.

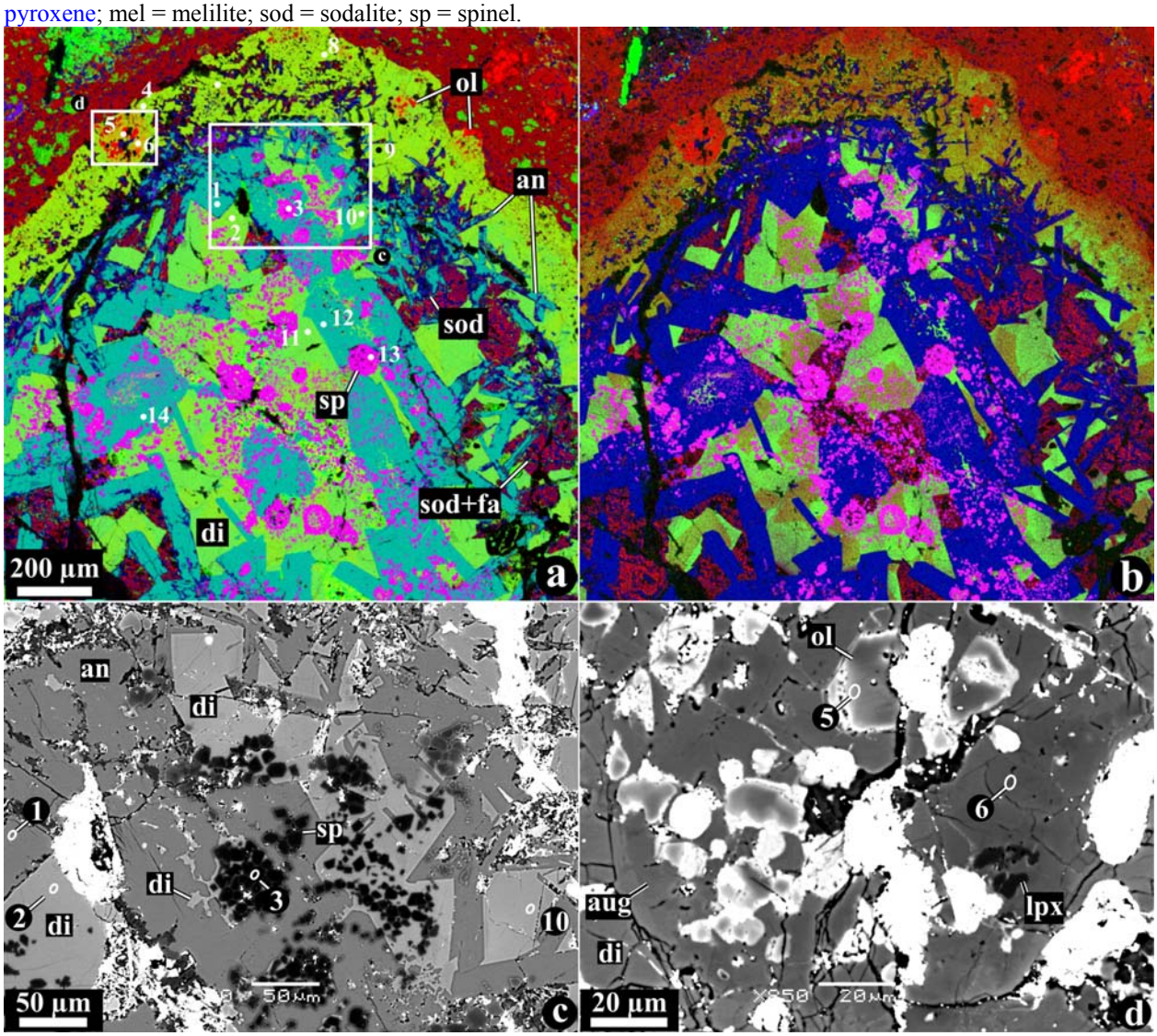

Fig. 14. a, b - Oxygen isotopic compositions of secondary magnetite (Mgt) and fayalite (Fa) in type I chondrules in the oxidized Bali-like CV chondrites Mokoia and Kaba (data from Choi et al., 2000; Hua et al., 2005; the latter are labeled by "*" in the legend to "b"). c, d - Oxygen isotopic compositions of secondary magnetite, Ca,Fe-pyroxenes (CaFe-px) and andradite (Andr) in various Allende components. Data for magnetite from Choi et al. (2000); data for Ca,Fe-pyroxenes, fayalitic olivine and andradite from Krot et al. (2000) and Cosarinsky et al. (2003). Error bars are 2σ.

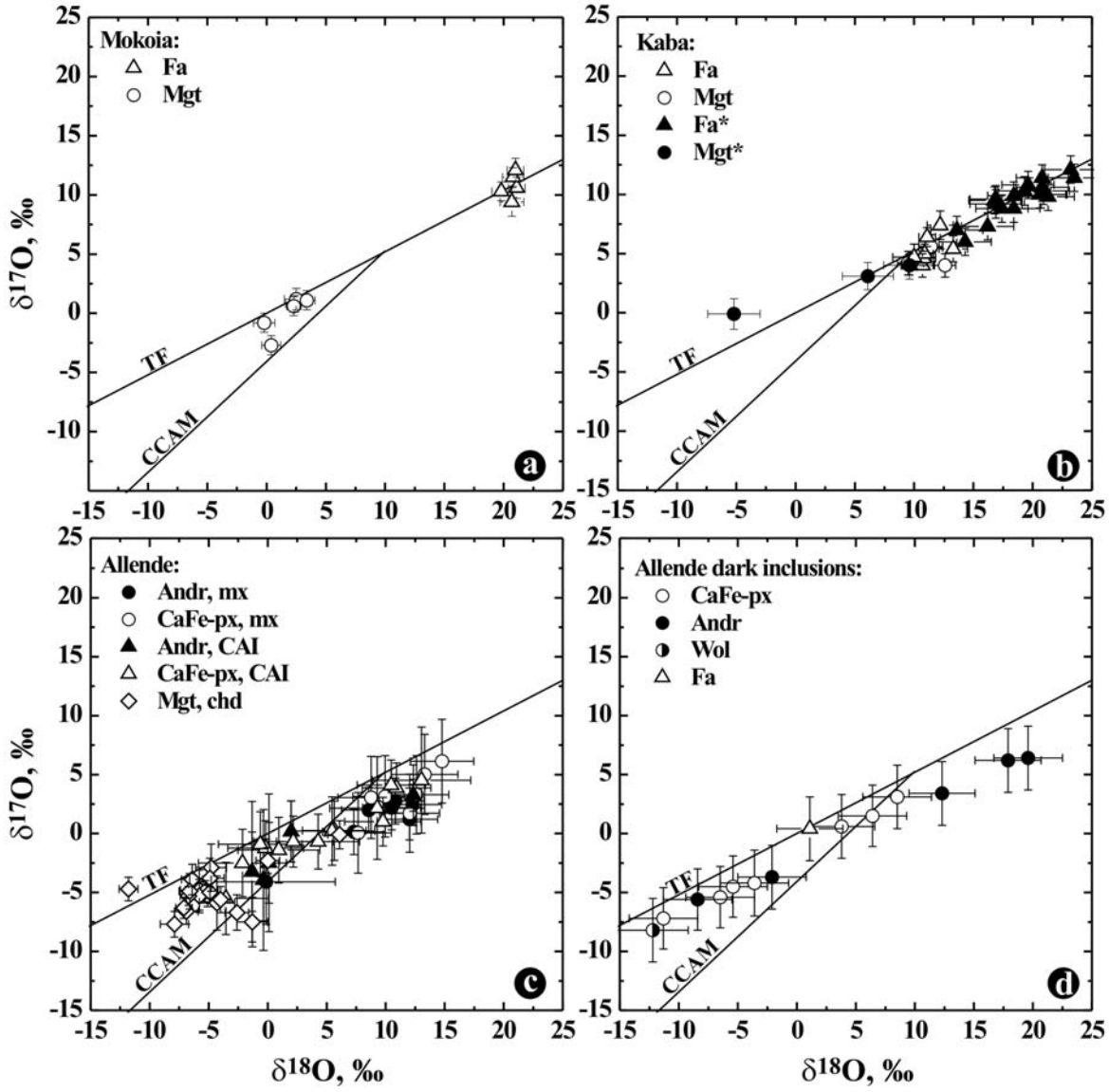

Fig. 1EA. (a) Combined elemental maps in Mg (red), Ca (green) and Al (blue) Kα X-rays and (b) elemental map in Ti Kα X-rays of a Type C *160*. an = anorthite; di = Al,Ti-diopside; fgr = fine-grained rim; fsl = ferrosilite; hed = hedenbergite; mel = melilite; mnl = monticellite; nph = nepheline; sod = sodalite; sp = spinel; WLR = Wark-Lovering rim.

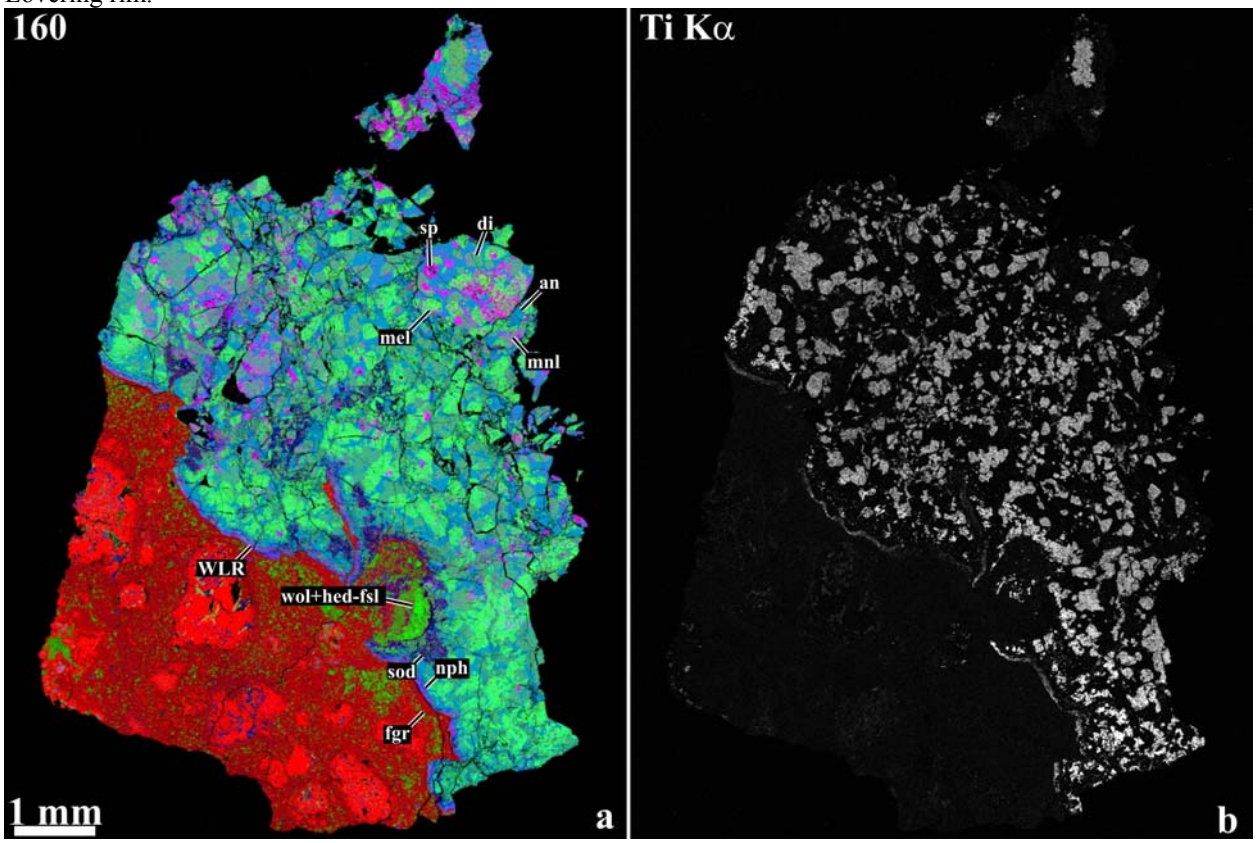

Fig. 2EA. Combined elemental maps in Mg (red), Ca (green) and Al (blue) Kα X-rays of four fragments ("*100a*", "*100b*", "*100c*", and "*100c*") of a Type C *100*. an = anorthite; di = Al,Ti-diopside; grs = grossular; mel = melilite; mnl = monticellite; nph = nepheline; sp = spinel.

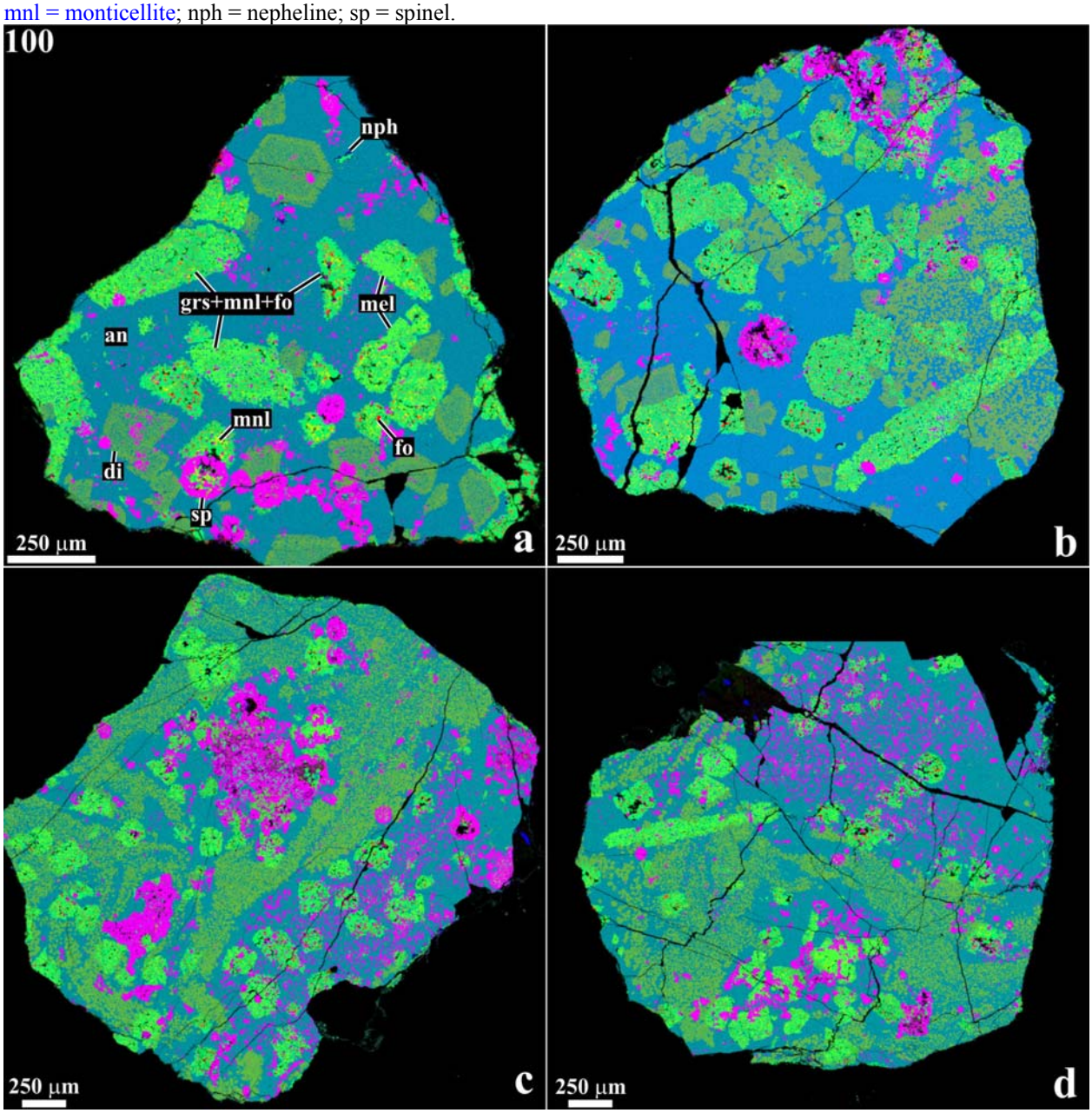

Fig. 3EA. (a) Combined elemental maps in Mg (red), Ca (green) and Al (blue) Kα X-rays and (b) elemental map in Ca Kα X-rays of a Type C *61-72*. an = anorthite; di = Al,Ti-diopside; mel = melilite; nph = nepheline; ol = olivine; sod = sodalite; sp = spinel. The CAI consists of two mineralogically distinct portions: Type B-like and Type C.

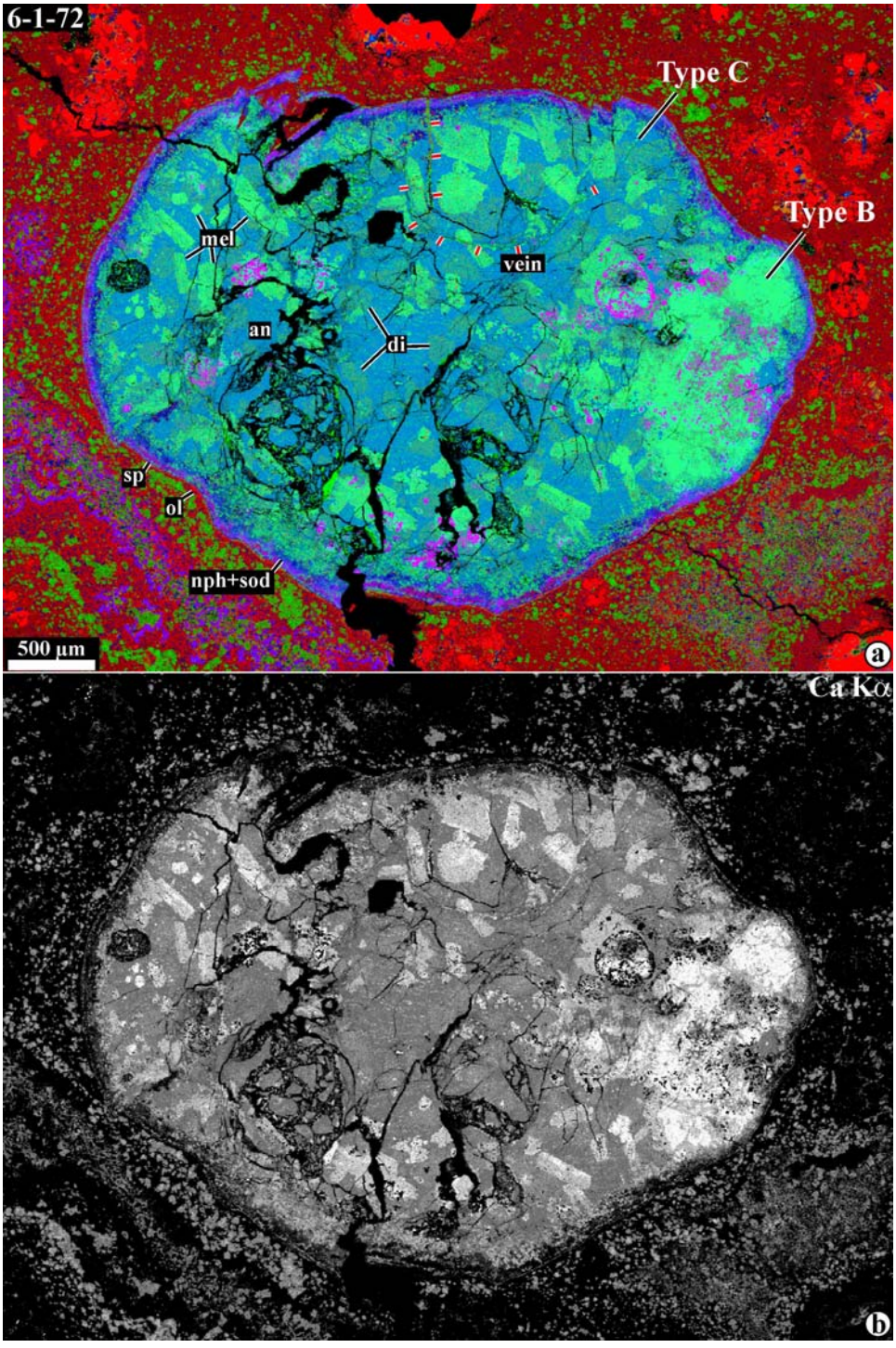

Fig. 4EA. (a) Combined elemental maps in Mg (red), Ca (green) and Al (blue) Kα X-rays and (b) elemental map in Ti Kα X-rays of a Type C *CG5*. an = anorthite; di = Al,Ti-diopside; mel = melilite; sp = spinel.

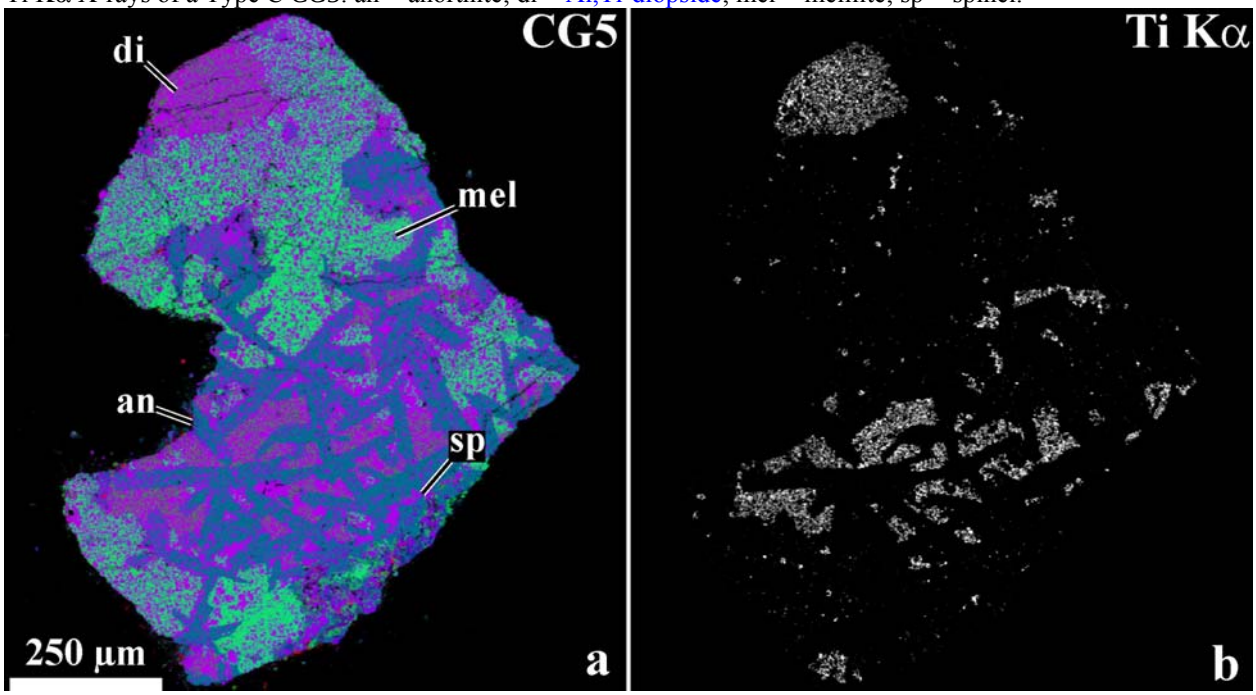

Fig. 5EA. (a) Optical micrograph in cross-polarized transmitted light and (b) combined elemental maps in Mg (red), Ca (green) and Al (blue) Kα X-rays of a Type C *TS26*. Arrows in "b" indicate relict chondrule fragments in the CAI mantle.